Design and development of stapled transmembrane peptides that disrupt the activity of G-protein coupled receptor oligomers

Joaquín Botta[1,2], Lucka Bibic[2], Patrick Killoran[3], Peter J. McCormick*[1] and Lesley A. Howell*[4]

From the [1]Centre for Endocrinology, William Harvey Research Institute, Bart's and The London School of Medicine and Dentistry, Queen Mary University of London, Charterhouse Square, London, EC1M 6BQ; [2]School of Pharmacy, University of East Anglia, Norwich Research Park, Norwich, NR4 7TJ; [3]School of Pharmacy and Biomolecular Sciences, James Parsons Building, Byrom Street, Liverpool, L3 3AF; [4]School of Biological and Chemical Sciences, Queen Mary University of London, Mile End Road, London, E1 4NS

Running Title: *Stapled TM peptides modulate GPCR oligomers*

* To whom correspondence should be addressed: Lesley A. Howell: School of Biological and Chemical Sciences, Queen Mary University of London, Mile End Road, London, E1 4NS; l.howell@qmul.ac.uk; Tel. (+44) 207 8826625 or Peter J. McCormick: Centre for Endocrinology, William Harvey Research Institute, Bart's and The London School of Medicine and Dentistry, Queen Mary University of London, Charterhouse Square, London, EC1M 6BQ; p.mccormick@qmul.ac.uk.

Keywords: G protein-coupled receptor (GPCR), cannabinoid receptor type 1 (CB_1), dimerization, cell-penetrating peptide (CPP), peptide chemical synthesis, serotonin receptor type 2A ($5HT_{2A}$), NanoLuc binary technology (NanoBiT), hydrocarbon stapling, transmembrane peptide, bimolecular fluorescence complementation

ABSTRACT

Membrane proteins can associate into larger complexes. Examples include receptor tyrosine complexes, ion channels, transporters and G-protein coupled receptors (GPCRs). For the latter, there is abundant evidence indicating that GPCRs, assemble into complexes, through both homo or heterodimerization. However, the tools for studying and disrupting these complexes, GPCR or otherwise, are limited. Here we have developed stabilized interference peptides for this purpose. We have previously reported that tetrahydrocannabinol-mediated cognitive impairment arises from homo- or hetero-oligomerization between the GPCRs cannabinoid receptor type 1 (CB_1R) and 5-hydroxytryptamine 2A ($5\text{-}HT_{2A}R$) receptors. Here, to disrupt this interaction through targeting CB_1–$5\text{-}HT_{2A}$ receptor heteromers in HEK293 cells and using an array of biochemical techniques, including calcium and cAMP measurements, bimolecular fluorescence complementation assays, and CD-based helicity assessments, we developed a NanoLuc binary technology (NanoBiT)-based reporter assay to screen a small library of aryl-carbon–stapled transmembrane mimicking peptides produced by solid-phase peptide synthesis. We found that these stapling peptides have increased α-helicity and improved proteolytic resistance without any loss of disrupting activity *in vitro,* suggesting that this approach may also have utility *in vivo*. In summary, our results provide proof of concept for using NanoBiT to study membrane protein complexes and for stabilizing disrupting peptides to target such membrane complexes through hydrocarbon-mediated stapling. We propose that these peptides could be developed to target previously un-druggable GPCR heteromers.

The discovery that G-protein coupled receptors (GPCRs) could oligomerize, termed homo or heterodimerization, sparked an intense

debate that has moved on from not if they can but to why, how, how frequently and how do we target them for therapeutic purposes. Several X-ray resolved GPCRs crystal structures have revealed common dimeric interfaces stabilizing oligomeric arrangements within the Rhodopsin-like family receptors. Dimers having an interface involving the transmembrane (TM) domains TM1, TM2 and H8 appear to be a commonly conserved organization, including the structures of the rhodopsin, opsin, metarhodopsin II, μ and κ opioid, and the β1 adrenergic receptors (1–6). An additional interface involving the TM4 and TM5 domains was also shown in the squid rhodopsin and the β1 adrenergic receptors (2, 7). Furthermore, the crystal structures of the CXCR4 and μ-opioid receptors revealed a substantial buried surface area of 850 $Å^2$ and 1,492 $Å^2$, respectively, comprised of the TM5 and TM6 domains (3, 8). Selective disruption of dimers using synthetic peptides harbouring the same amino acid sequence as the interacting TM domains, has helped to validate and understand the functional consequences of receptor oligomerization, including the β2 adrenergic, CXCR4, oxytocin and apelin receptors homo-oligomers (9–12). Synthetic peptides have also provided unique tools to map the interfaces and understand the biological relevance of Class A GPCRs heteromerization (13, 14). An additional advantage of TM peptides is that, unlike knock-out studies or deletions, the peptides preserve the functional single protomers and allow one to discriminate between those effects driven by the interacting receptors and those derived from the individual protomers. An example of the former is the *in vivo* disruption of the cross-class angiotensin receptor subtype 1a (AT1aR) and secretin receptor heteromers with a TM1 AT1aR mimetic peptide, reducing hyperosmolality-induced drinking behaviour (13).

In cases where heteromer disruption might serve a therapeutic purpose, it would be advantageous to translate TM peptides not only as tools, but into drug-like entities. Peptides in general are considered poor drug like molecules, although this view is changing. Efficacy is often compromised *in vivo* due to a loss of secondary structure; cellular uptake is poor and finally peptides are highly susceptible to proteolysis. Stapling of the peptide backbone can help to overcome these limitations; the bioactive conformation of the peptide is maintained, and careful positioning and choice of staple can result in a high affinity binder with improved cellular uptake and stability. Stapled peptides therefore represent an attractive approach to developing more drug-like peptides. For a recent review on stapled peptides see Ali et al (15). We have previously shown that the undesired effect of cognitive impairment in the presence of trans-Δ9-tetrahydrocannabinol (THC) is driven by homo/hetero-oligomerization between CB_1 and 5-HT_{2A} receptors (16). To disrupt this interaction, we developed a NanoBiT-based assay for the screening of a small library of aryl-hydrocarbon stapled CB_1R TM5 mimicking peptides to target CB_1-5-HT_{2A} receptor heteromers. NanoBiT is a luciferase based complementation assay designed to interrogate protein-protein interactions in live cells (17). Using this approach we found that stapling peptides led to increased α-helicity and improved proteolytic resistance without any loss of function, suggesting this approach may improve these molecules chances *in vivo*.

Results

Establishing the NanoBiT system for heteromer screening purposes

The CB_1 and 5-HT_{2A} receptor heteromer has been recently characterized both *in vivo* and in heterologous expression systems using a broad range of biochemical approaches (16). In the case of these heteromers, the cognitive impairment induced by THC is abrogated after treatment with CB_1R TM5 peptides, while maintaining its antinociceptive properties (16). Therefore, for therapeutic purposes there needs to be prevention of heteromer formation but preservation of the individual protomer's function. Thus, we first sought to develop a NanoBiT-based assay for the screening of a small library of hydrocarbon stapled CB_1R TM5 mimicking peptides. To assess whether NanoBiT BiLC may be a suitable system to study GPCR oligomerization, we generated CB_1R and 5-HT_{2A}R constructs with the small and large BiT pairs (SmBiT and LgBiT, respectively) attached to the *C*-terminus end of both receptors. A total of four fusion proteins were generated, with Sm/LgBiT fused after the

Gly/Ser rich flexible linker and under the control of the herpes simplex virus thymidine kinase gene promoter (HSV-TK) (Figure S1A). Next, we performed conformational screenings to assess the optimal configuration for all receptor pairs. Accordingly, when analysing CB_1R-5-HT_{2A}R heteromers, HEK293 cells were transiently transfected with all possible combinations of 5-HT_{2A}R Lg/SmBiT and CB_1R Lg/SmBiT at two different DNA ratios (Figure S1B). Surprisingly, none of the analysed configurations yielded a positive interaction. Similarly, when addressing the formation of CB_1R and 5-HT_{2A}R homodimers, none of the examined orientations nor DNA ratios exhibit significant differences in comparison with the individual receptors when expressed by themselves (Figures S1C and D). Importantly, to rule out whether these negative results might reflect the unsuitability of the NanoBiT system for the analysis of GPCR oligomerization rather than any kind of experimental hindrance, we analysed the known interaction between the protein kinase A catalytic (PRKACA) and type 2A regulatory (PRKAR2A) subunits. This protein pair positive control has been previously optimized, with LgBiT-PRKAR2A and SmBiT-PRKACA the optimal configuration (17). In agreement, co-transfection of both proteins resulted in a significant increase in the luminescence recorded over the different receptor ratios. Furthermore, co-transfection of LgBiT-PRKAR2A with a non-interacting fusion protein (HaloTag®-SmBiT) did not yield any increase in luminescence (Figure S1E), supporting the specificity of the detected interaction and the suitability of this system under our assay conditions. However, our results do not rule out whether the complementary fusions restrict 5-HT_{2A}R or CB_1R functionality or if there is indeed a lack of complementation. Importantly, it should be noted that to minimise potential non-specific interactions all generated constructs were under the control of the HSV-TK promoter.

Thus, in order to address the lack of a BiLC signal, we performed secondary messenger signalling experiments and re-cloned all four receptor configurations under the control of the high-level expression cytomegalovirus (CMV) promoter. Interestingly, all 5-HT_{2A}R constructs in an HSV-TK context failed to elicit intracellular calcium release (canonical signalling pathway downstream to the $G_{q/11}$-coupled 5-HT_{2A}R) after agonist stimulation (18). However, both 5-HT_{2A}R-LgBiT and 5-HT_{2A}R-SmBiT displayed similar efficacies and potencies in comparison to the wild type (WT) receptor when expressed under the control of the CMV promoter (Figure S2A). Similarly, we assessed CB_1R-driven adenylate cyclase (AC) inhibition with analogous results. Both CMV-regulated CB_1R constructs inhibited the Forskolin (FK)-induced cAMP release with equivalent potencies and efficacies to the WT CB_1R receptor. However, under the HVS-TK promoter, CB_1R-LgBiT failed to signal through heterotrimeric $G_{i/o}$ proteins and CB_1R SmBiT exhibited a reduced AC inhibitory activity (~20%) when compared to WT CB_1R receptor (Figure S2B). These results indicate than the NanoBiT fusions do not adversely affect 5-HT_{2A} nor CB_1 receptor functionality, as the ligands potencies and maximal efficacies are within the wild type receptors ranges. Thus, the absence of luciferase complementation between HSV-TK regulated constructs most likely reflects low levels of receptor expression due to the weaker promoter, rather than steric hindrance of the interacting pairs (19).

NanoBiT can be used to estimate receptor affinities

Accordingly, as in the previous studies illustrated in Figure 1A, we repeated the conformational screenings with the new set of constructs under the CMV promoter. When analysing 5-HT_{2A}R-CB_1R heteromerization, we detected a significant increase in the luminescence for all receptor combinations, with 5-HT_{2A}R-LgBiT:CB_1R-SmBiT being the optimal pair in terms of assay window (Figure 1B). To validate the specificity of the interaction, increasing amounts of untagged 5-HT_{2A}R and CB_1R receptors were transfected in the presence of a fixed 5-HT_{2A}R-LgBiT:CB_1R-SmBiT ratio. Accordingly, we observed a decreased luminescence with increasing levels of both untagged proteins (Figures 1E and F), indicating that the detected interaction was not driven by the finite affinity between the

NanoLuc subunits. In parallel, we assessed CB_1R and 5-$HT_{2A}R$ homomerization with similar results. Co-transfection of both CB_1R interacting pairs resulted in a significant increase in luminescence that could be reverted by increasing untagged CB_1R concentrations (Figures 1C and G). Similarly, the specific interaction between 5-$HT_{2A}R$-LgBiT and 5-$HT_{2A}R$-SmBiT was hindered when titrating increasing concentrations of untagged 5-$HT_{2A}R$ (Figures 1D and H). Importantly, when comparing the relative intensities of these interactions, we found that 5-$HT_{2A}R$ homodimers displayed the highest luminescent signals, followed by 5-$HT_{2A}R$-CB_1R heteromers and CB_1R homodimers (RLU for 5-$HT_{2A}R$:5-$HT_{2A}R$ > 5-$HT_{2A}R$:CB_1R > CB_1R:CB_1R). In addition, higher non-tagged 5-$HT_{2A}R$ concentrations were necessary to displace 5-$HT_{2A}R$ homodimers (Figure 1H). However, our results cannot discriminate whether it reflects the relative affinities between the interacting receptors or a more proximal distance of the NanoBiT pairs in the C-terminus of the receptors. Altogether, our data strongly supports NanoBiT BiLC as a non-destructive and powerful tool to study GPCRs oligomerization, providing a specific and sensitive assay to detect these receptor complexes in live cells.

Comparison of NanoBiT with Venus bimolecular fluorescent complementation

In order to obtain a more comprehensive understanding of bimolecular complementation assays to study GPCR oligomerization, we sought to address whether NanoBiT could provide better results in comparison to bimolecular fluorescent complementation. To this end, we developed a Venus BiFC assay to study CB_1R and 5-$HT_{2A}R$ homo/heteromerization. Specifically, fragments derived from the truncated Venus fluorescent protein at either position D155 (VC155; amino acid residues 155 to 238) or D173 (VN173; amino acid residues 1 to 173) where fused after the Gly/Ser rich flexible linker to the C-terminus of both CB_1 and 5-HT_{2A} receptors (Figure 2A). This strategy has been extensively applied to the study of protein-protein interactions (PPIs) and takes advantage of Venus, a variant of the enhanced yellow fluorescent protein (eYFP) with improved sensitivity to chromophore maturation under physiological temperatures (21). Several groups have used this approach to study GPCR oligomerization, including heteromers between the adenosine A_{2A} ($A_{2A}R$) and the dopamine D_2 (D_2R) receptors, D_2R oligomers or neuropeptide Y Y_1/Y_5 receptor heterodimers (19–21).

Attachment of both Venus hemiprotein fragments to the 5-$HT_{2A}R$ C-terminal tail (5-$HT_{2A}R$-VN173 and 5-HT_{2AR}-VC155 constructs) did not impact receptor function, with equivalent $[Ca^{2+}]_i$ release dose-response curves in comparison to the wild type receptor (Figure S3A). Similarly, the VC155 fragments fused to CB_1R (CB_1R-VC155) did not affect CB_1R-mediated cAMP release inhibition. However, although its maximal efficacy remained unaltered, VN1733 fusion to CB_1R (CB_1R-VN173) resulted in ~10-fold reduction in WIN 55212-2 (WIN) potency (Figure S3B). Next, we proceeded to compare both protein complementation assays. For CB_1R and 5-$HT_{2A}R$ homomers, BiFC experiments were performed under the same conditions that yielded the optimal assay windows in the NanoBiT BiLC experiments (Figure 2). When assessing 5-$HT_{2A}R$-CB_1R heteromers, both possible receptor configurations (5-$HT_{2A}R$-VN173:CB_1R-VC155 or 5-$HT_{2A}R$-VC155:CB_1R-VN173) were taken into account. Surprisingly, 24 and 48 hours after reverse transfection, none of the analysed BiFC combinations yielded significant fluorescent levels (data not shown), suggesting time-dependent protein maturation and/or folding. Therefore, the following BiFC experiments were performed 48 hours post-transfection (see methods section), although BiLC assays remained under the same setup (24 hours post-transfection). In comparison to Venus BiFC, NanoBiT complementation provided higher assay windows over all the oligomeric configurations (Figure 2). Specifically, we observed a 20-fold increase for CB_1R homodimers, 130-fold increase for 5-$HT_{2A}R$ homodimers and 9-18-fold increase for 5-$HT_{2A}R$-CB_1R heteromers. Interestingly, the relative fluorescent/luminescent intensities for the different receptor pairs followed the same

trend across both methods (RFU/RLU for 5-HT_{2A}R:5-HT_{2A}R > 5-HT_{2A}R:CB_1R > CB_1R:CB_1R), suggesting that this could reflect the affinity between these oligomeric arrangements.

N-terminal GPCR fusions are also functional for NanoBiT complementation

Next, we sought to test whether N-terminal tagging might yield better assay windows (Figure 3A). SmBiT and LgBiT fusion to the 5-HT_{2A}R extracellular end did not impact function as treatment with the agonist DOI induced maximal calcium release, although a small reduction in DOI potency was observed in the LgBiT-5-HT_{2A}R construct (Figure S4A). The homologous CB_1R constructs remained unaltered, with virtually the exact potencies and maximal responses as the WT receptor (Figure S4B). Next, we compared *N*- or *C*-terminal NanoBiT-tagged receptors accounting for their ability to reveal CB_1R and 5-HT_{2A}R homo/heteromers. When measuring the interaction between receptors from the same type, NanoBiT attachment to the *C*-terminal domain provided the optimal orientation for CB_1R homomers (Figure 3B). In the case of 5-HT_{2A}R homomers, *N*-terminally tagging resulted in a discrete but significant improvement in the assay window at high DNA concentrations (Figure 3B). Interestingly, the biggest difference was observed when assessing the optimal 5-HT_{2A}R-CB_1R heteromeric conformation, with the *N*-terminal fusions providing the best results (Figure 3C). Importantly, a ~200-fold increase was achieved at low DNA transfected concentrations, therefore reducing the probability of stochastic non-specific interactions and thus more closely mimicking physiological expression levels. The LgBiT-CB_1R and SmBiT-5-HT_{2A}R combination was therefore used in all further experiments.

Design and synthesis of stapled peptides

In previous studies, we demonstrated that 5-HT_{2A}R-CB_1R heteromers could be selectively disrupted using synthetic peptides mimicking the CB_1R TM5 and TM6 domains (16), fused to the HIV-TAT (GRKKRRQRRR) cell penetrating amino acid sequence (CPS) (23). In the same study we also showed that the peptide mimicking CB_1R TM7 did not disrupt the heteromer. As part of our preliminary work, we had previously identified a truncated CB_1R TM5 amino acid sequence fused to TAT (VYAYMYILWGRKKRRQRRR) capable of disrupting the 5-HT_{2A}R-CB_1R heteromer (unpublished). We therefore chose to design stapled peptides based on the amino acid sequences of the truncated CB_1R TM5 to aid with the synthesis and purification of the peptides as well as solubility. In addition, amino acid sequences of 20-25 amino acid residues or less are generally recommended for stapling (24)

Accordingly, using these structures as a starting point, we hypothesized that shortening their length, in combination with hydrocarbon peptide stapling, could result in peptides with more drug-like properties. (Figure 4A). This strategy, through the incorporation of α-methyl-α-alkenyl amino acids, combines the methylation of the α-carbon atom together with the introduction of a covalent side chain to side chain cross-link, resulting in peptides with increased α-helicity and improved proteolytic resistance (25, 26). We next evaluated where to add the hydrocarbon staples. One major consideration is charge. An overall positive net charge is favourable after staple installation to aid with cellular uptake. The location of the positive amino acids is also influential and if possible should be located at the *C*-terminus. Molecular modelling identified potential sites within these TM5 peptide amino acid sequences to introduce the hydrocarbon staple (Table 1). The positions (facing the membrane of CB_1R) to build the stapled peptides (at i and i+3/4) are shown in red. The TAT amino acid sequence is shown in orange.

Peptides are often thought of as poor drug molecules as; 1) *in vivo* their efficacy is compromised due to a loss of secondary structure; 2) they often have poor cellular uptake and 3) they are highly susceptible to proteolysis. Stapling of the peptide backbone is an attractive strategy to overcome these limitations; the bioactive conformation of the peptide is maintained, and careful positioning and choice of staple can result in a high affinity binder with improved cellular uptake and stability. Next, is the choice of staple to use. We chose to incorporate the all-hydrocarbon

staple for alpha-helical peptide stabilization. This was first reported in 2000 by Schafmeister et al. (27) and has since found use in a variety of applications including cancer, infectious diseases and neuroscience (28). In addition, this staple has been shown to protect the peptide against proteolysis as the vulnerable peptide bonds are sequestered in the interior of the helix. The building block for single turn hydrocarbon stapling is the unnatural amino acid *S*-pentenylalanine (Fmoc-S_5-OH). Although available commercially, we chose to synthesise the Fmoc-protected version in-house adapting methods reported by Jamieson and Ryzhov (scheme 1) (29, 30). Briefly, *N*-alkylation of proline with 2-fluorobenzyl bromide gave **1** in almost quantitative yields. This was followed by the condensation of **1** with 2-aminobenzophenone to give the chiral auxiliary (*S*)-*N*-(2-benzoylphenyl)1(2-fluorobenzyl)-pyrrolidine-2-carboxamide **2** (2-FBPB). Complexation with nickel nitrate and L-alanine gave (*S*)-Ni-Ala-2FBPB **3** in almost quantitative yields. This was followed by asymmetric alkylation to yield complex **4** in a good yield which was subsequently decomposed under acidic conditions to give *S*-pentenylalanine **5**. Finally, this was Fmoc protected by reaction with Fmoc chloride under basic conditions to afford Fmoc-*S*-pentenylalanine **6**. Following synthesis of the unnatural amino acid we turned our attention to the synthesis of the CB_1R TM5 peptides.

Five peptides (**7**-**11**) were designed for our study including one negative control (**11**) (Figure 4A). Methionine amino acid residues were replaced with norleucine amino acid residues to avoid any complications or unwanted side reactions during ring closing metathesis reactions. Peptides were synthesised using Fmoc-based solid-phase peptide synthesis (SPPS) using procedures reported previously (9). Scheme 2 outlines an example synthesis. During assembly the Fmoc-S_5-OH is incorporated into positions separated by 2 or 3 amino acid residues as shown in Figure 4A. Coupling times were increased from 45 minutes to 60 minutes for the Fmoc-S_5-OH and for the residue following the olefinic unnatural amino acid. The assembled peptides (**7**-**10**) were then subjected to the ring-closing metathesis (RCM) reaction whilst still on the solid support. This was monitored using reversed-phase high performance liquid chromatography (RP-HPLC); note peptide **7** did not undergo the RCM reaction. Following a final Fmoc deprotection step, the stapled peptides were cleaved from the solid support under acidic conditions and subsequently purified using preparative RP-HPLC and freeze dried from water as previously described (30). The negative control **11** was treated in an identical fashion with the exception that the RCM step was omitted. Purified peptides were analysed using analytical RP-HPLC to assess purity and matrix assisted laser desorption ionisation-time of flight (MALDI-TOF) mass spectrometry to determine accurate mass. All peptides were soluble in water/aqueous buffer.

The administration of peptides to disrupt GPCR interactions is relatively new, with no available information regarding their pharmacokinetics and/or pharmacodynamics. Often with peptides, the *in vivo* efficacy is compromised due to a loss of secondary structure; to assess the helicity of the peptides and whether incorporation of the staple had increased the helical nature of the peptides we employed circular dichroism spectroscopy. (Figure 4B). CB1 TM5-TAT, TM6-TAT and TM7-TAT all displayed relatively low helicity in solution (less than ~20%). Pleasingly, incorporation of the staples increased the helical nature of the stapled peptides **8-10** in all cases when compared to the TM5-TAT peptide. Peptide **8** demonstrated the highest helicity of 58.3%. Interestingly the negative control **11**, where the olefinic amino acids are present but not stapled, displayed an almost identical helicity (46.0%) when compared with the stapled version **9**. When TAT is added to the amino acid sequence **10**, the helicity drops slightly to 36.8%. A second challenge facing protein/peptide therapies is proteolytic degradation. Consequently, we subjected our peptide library to *in vitro* trypsin, chymotrypsin and serum proteolytic stability. When monitoring trypsin (0.55 μg/mL) degradation kinetics (Figure 4E), a rapid proteolysis was observed for the TM7-TAT, TM6-TAT and TM5-TAT control peptides (55 μM each), with half-lives ranging from 20-40 minutes.

Pleasingly, the short-stapled CB_1R TM5 amino acid sequence harbouring the TAT amino acid sequence **10** displayed a longer half-live, with a 2-3-fold enhancement in trypsin resistance. Furthermore, removal of the TAT amino acid sequence in the stapled peptides (**8**,**9**) yielded the longest half-lives (~5 hours), as neither lysine nor arginine amino acid residues were available for the trypsin to cleave. This increase in half-life was also observed for the negative controls where the TAT amino acid sequence was removed. Chymotrypsin proteolytic kinetics showed similar results (Figure 4F); the full length TM7-TAT, TM6-TAT and TM5-TAT peptides were more susceptible to cleavage (half-lives ranging from 20 to 30 min). Again, a ~2-fold resistance improvement was detected for stapled peptide **10** bearing the TAT amino acid sequence. Likewise, **8** and **9** were the peptides with longer half-lives (5-6 hours) (Figure 4F**).** In mouse serum, a more physiologically relevant context, the TM7-TAT, TM6-TAT and TM5-TAT peptides were rapidly degraded, with a 1-hour incubation sufficient to break down 50% of them (Figure 4G). Hydrocarbon stapling translated to an even higher serum stability in comparison with trypsin and chymotrypsin, with peptides **8** and **9** displaying half-lives of more than 10 hours. These results positively correlate with the respective helicity of each peptide, as the reinforcement of α-helical structure limits the peptides to adopt the extended conformation required by proteases to hydrolyse the amide bonds (25). Accordingly, we observed a strong positive correlation between helicity and proteolytic resistance (r=0.84, 0.78 and 0.87 for trypsin, chymotrypsin and mouse serum, respectively; Figures 4C and D). Finally, we investigated the effects of the peptides on cell proliferation and toxicity using a Label-Free assay. Specifically, we analysed cell viability based on changes in electrical impedance over time. No statistically significant reduction in viability of the cells was observed over a 24 or 48h period (Figure S5).

Stapled peptides are effective at disrupting heteromers

Next we sought to test whether stapling changed the ability of the peptides to disrupt GPCR heteromers (schematic in Figure 5A). Pre-incubation of HEK293 cells transiently co-expressing $LgBiT\text{-}CB_1R$ and $SmBiT\text{-}5\text{-}HT_{2A}R$ with the TM5-TAT and TM6-TAT, but not the TM7-TAT (negative control) peptides resulted in a decrease in the luminescence readout (Figure 5B), corroborating the previously reported results demonstrating the involvement of TM5 and TM6, but not TM7, in the heteromeric interface (16). In addition, these results demonstrate the suitability of our NanoBiT-based peptide screening assay and the specificity of the detected interaction.

Next we tested whether the stapled versions were as efficient at blocking heteromerization (Figure 5B). When analysing the TM5-TAT-derived peptides, compound **10** exerted a significant decrease in NanoBiT complementation. Interestingly however, neither the version lacking the TAT amino acid sequence, compound **9**, nor the non-staple, compound **11**, peptides induced any change. It was not simply length of the peptide, as the longer stapled compound **8** also was not as efficient as compound **10** at disrupting the complex. Stapling in itself did not seem to convey an advantage as comparing compounds **9** and **11**, we observed equal effects.

We next sought to understand the disruption efficacy and the timing of compound **10**'s effects on the heteromer. Treatment with increasing concentrations of compound **10** induced a dose-dependent luminescence decrease, with a potency in the low micromolar range (pIC_{50} = 5.47 ± 0.01) (Figure 5C). Surprisingly, the ability of compound **10** to disrupt $5\text{-}HT_{2A}R\text{-}CB_1R$ heteromers was on the order of minutes, reaching its maximal inhibitory response approximately five minutes after administration (Figure 5D).

Altogether, by developing a sensitive and specific bimolecular luminescent complementation assay we were able to screen a small library of peptides targeting $5\text{-}HT_{2A}R\text{-}CB_1R$ heteromers. In addition, covalent side chain to chain cross-linking through hydrocarbon peptide stapling lead us to the identification of a small TM peptide mimetic, **10**, with improved stability, helicity and efficacy.

Discussion

Here we have successfully provided a proof of concept for two new tools to study GPCR oligomerization. First, we successfully applied the recently developed NanoLuc binary technology (NanoBiT) to study GPCR oligomerization. Using this system, we validated the previously demonstrated association of CB_1R and 5-HT_{2A} receptors as homodimers and their ability to form heteromers (16, 31, 32). Second, we have demonstrated that interference peptides can be dramatically stabilised and shortened using aryl-carbon stapling. These two advances will prove useful in studying GPCR oligomerization both *in vitro* and particularly *in vivo*.

When adapting the NanoBiT to study oligomerization we predicted that the small size of the complementary fragments (18kDa and 1.3 kDa for LgBiT and SmBiT, respectively), would minimize steric conflicts (17). In fact, agonist potencies and maximal efficacies were equivalent to their matched wild type receptors under the same promoters. Apart from GLuc (19 kDa), NLuc (19 kDa) is significantly smaller in comparison to other fluorescent/luminescent proteins used in resonance energy transfer (RET) or protein complementation assays (ranging from 26 kDa for YFP up to 61 kDa for FLuc). In addition, no post-translational modifications have been reported in mammalian cells, resulting in lower energetic costs in terms of translation, sorting and proper polypeptide folding. Accordingly, our initial studies were performed under the control of the low copy number herpes simplex virus thymidine kinase gene promoter (HSV-TK)(19). However, under this configuration, we were not able to quantitatively assess agonist-induced downstream signalling pathways. Importantly, most DNA constructs for FRET/BRET and BiFC assays use transient expression systems such as pcDNA3.1 vectors, with the cDNA expressed under the control human cytomegalovirus (CMV) immediate-early enhancer and promoter (33, 34). Using this strategy, we developed a microtiter-based homogeneous assay that allowed the identification of GPCRs oligomers in just 24 hours, reducing the chance of over-expression-related non-specific interactions. When comparing our NanoBiT-based dimerization assay with Venus YFP BiFC, an approach used to visualize more than 200 PPIs, including many GPCR homo/heteromers (22), NanoBiT BiLC proved far more sensitive at detecting CB_1R and 5-$HT_{2A}R$ homodimers and 5-$HT_{2A}R$-CB_1R heteromers. Presumably, the small size of the fused fragments, NanoLuc high quantum yield and the lack of BiFC maturation step act synergistically to allow us to detect PPIs 24 hours after transfection under physiological conditions. More recently, TANGO and SPARK have been developed to study PPIs (35, 36). Both are good approaches for larger screens or in the case of SPARK enrichment of cell populations by fluorescence-activated cell sorting (FACS). The NanoBiT system adapted here is good for studies directly interrogating the interactions themselves, say for mapping the interactions themselves or testing known small molecules as we have shown in this study. Previously a split NanoLuc system was published to study G-protein signalling but it does not have the advantage of having a short peptide portion on one of the partners as is used in the NanoBiT system(37).

Interference peptides have been used in multiple studies to validate or disrupt GPCR heteromers (9, 13, 16, 38, 39). However, these peptides often suffer from poor pharmacokinetics and have a poor chance of being used or developed into drug-like entities. To improve on the potential of such entities to be adapted as potential therapeutics we have stabilised a disrupting peptide using hydrocarbon stapling. This approach has been used on a variety of peptide therapeutics. However, to our knowledge stapled peptides have not been applied to G-protein coupled receptor oligomers. We demonstrate here that stapling of disrupting peptides can significantly shorten the required length of the peptide and dramatically improve the stability of the

peptides. These data support further development of such an approach to target GPCR oligomers *in vivo*.

An additional challenge presented in targeting such complexes is that the same membrane polypeptide can often interact with multiple partners in different complexes, eg. Dopamine 2 receptor can interact with A2a receptor as well as Dopamine 1 receptor, or different NMDA subunits or AMPA subunits can make up multiple complexes. To date, we have not seen that disrupting peptides are specific for a given complex. Our evidence here that additional modifications can be made to these peptides provide an opportunity for adding additional chemical modifications that might provide more complex specificity in the future.

Experimental procedures

1. Reagents

Unless stated otherwise, reagents and solvents were purchased as high-grade commercial products from Sigma-Aldrich. (R)-(+)-WIN 55212 (WIN) and (±)-2,5-Dimethoxy-4-iodoamphetamine hydrochloride (DOI) were purchased from Tocris Bioscience.

2. Expression vectors and cloning

Plasmids encoding the 3xHA-tagged human 5-HT_{2A} and CB_1 receptors were obtained from the cDNA Resource Center (#HTR02ATN01 and #CNR010TN01, respectively; www.cdna.org). Plasmids encoding the pGloSensor™-22F cAMP biosensor and the complementary NanoBiT pairs (pBiT1.1-C[TK/LgBiT], pBiT2.1-C [TK/SmBiT], pBiT1.1-N[TK/LgBiT], pBiT2.1-N[TK/SmBiT], LgBiT-PRKAR2A Control Vector, SmBiT-PRKACA Control Vector and NanoBiT® Negative Control Vector) were purchased from Promega. The pGP-CMV-GCaMP6s calcium sensor was a gift from Douglas Kim & GENIE Project (Addgene plasmid #40753). Plasmids encoding the Venus YFP complementary pairs pBiFC-bFosVC155 and pBiFC-bJunVN173 were a gift from Chang-Deng Hu (Addgene plasmids #22013 and #22012, respectively). All constructs generated in this study were generated following the Gibson assembly method according to the manufacturer's instructions (Gibson Assembly® Master Mix, NEB). Detailed information is provided in table S1. The correct assembly of the full genes was verified by Sanger sequencing using universal T7 FW 5'-TAATACGACTCACTATAGGG-3' and BGH RV 5'-TAGAAGGCACAGTCGAGG-3' primers for constructs in pcDNA3.1(+) backbone, FW 5'-TTGGCAATCCGGTACTGTTGG-3' and RV 5'-GCAATAGCATCACAAATTTC-3' primers for constructs in pBiT1.1-C [TK/LgBiT] and pBiT1.1-N [TK/LgBiT] backbones and FW 5'-TTGGCAATCCGGTACTGTGG-3' and RV 5'-GCAATAGCATCACAAATTTC-3' primers for constructs in pBiT2.1-C [TK/SmBiT] and pBiT2.1-N [TK/SmBiT] backbones.

3. Cell culture and transfection

Human embryonic kidney 293 (HEK 293) cells (ATCC® CRL-1573™) were grown in Dulbecco's modified Eagle's medium supplemented with 2 mM L-glutamine, 4.5 g/L D-glucose, 100 µg/mL sodium pyruvate, 100 U/mL penicillin, 100 µg/mL streptomycin and 10% (v:v) heat inactivated fetal bovine serum (Pan Biotech, Germany) at 37°C in a 5% CO_2 humidified atmosphere. Cells were directly transfected in 96-well plate format following the reverse Lipofectamine™ 3000 (Thermo Fisher) transfection method. Briefly, for each well, 100-200 ng of DNA and 0.2-0.4 µL of P3000™ reagent (1:2 w:v DNA:P3000/Lipofectamine™ 3000 ratio) were combined in 25 µL of Opti-

MEM® media. The total amount of DNA/well was kept constant with empty vector (pcDNA3.1). In a separate tube, 0.2-0.4 µL of Lipofectamine™ was added to 25 µL of Opti-MEM® media. Both reaction mixes were vortexed (2-5 sec) and incubated at RT for 5 min. After this time, the diluted DNA was added dropwise to the Lipofectamine™-containing tube, gently mixed by pipetting up and down and incubated for 15 min at RT. In parallel, cells were trypsinised according to standard mammalian tissue culture protocols and resuspended in complete cell culture media to $5 \cdot 10^5$ viable cells/mL. 100 µL of the cell suspension was distributed into each well and 50 µL of the transfection mix was added on top of the cells. The plates were then incubated at 37°C in a 5% CO_2 humidified atmosphere for 24-48 hours before performing the experiments.

4. Ca^{2+} and cAMP measurement

For $[Ca^{2+}]_i$ release quantification, 50,000 cells/well were reverse transfected (see above) with 50 ng/well of pGP-CMV-GCaMP6s calcium sensor vector and 100 ng/well of receptor in poly-D-lysine coated black clear bottom 96-well plates. 24 hours post-transfection, the cell culture medium was removed and the cells were starved in FBS-free DMEM for 4 hours at 37°C in a 5% CO_2 humidified atmosphere. Prior to $[Ca^{2+}]_i$ release measurements, the cell culture medium was replaced by 175 µL of Ca^{2+} assay buffer (145 mM NaCl, 2.5 mM KCl, 10 mM glucose, 10 mM HEPES, 2 mM $CaCl_2$, 1 mM $MgCl_2$; pH 7.4) and the plates were pre-equilibrated for 1 hour in the dark at 37°C in a 5% CO_2 humidified atmosphere. Immediately following agonist addition (25 µL, 8X final concentration), fluorescence emission intensity was recorded at 515 nm upon excitation at 488 nm in a CLARIOstar® Multimode Plate Reader (BMG Labtech, Germany) for 300 secs every 5 sec and 40 flashes/well at 37°C. To account for differences in expression/cell density, an average of 5 pre-readings were used to normalise each well's response.

cAMP measurements were performed as previously described (40). Briefly, 24 hours post-transfection, cells were incubated in FBS-free DMEM for 4 hours at 37°C in a 5% CO_2 humidified atmosphere. Prior to cAMP measurements, the cell culture medium was replaced and plates were pre-equilibrated for 1 hour with cAMP assay buffer (HBSS with 24 mM HEPES, 3.3 mM $NaHCO_3$, 1.3 mM $CaCl_2$, 1 mM $MgSO_4$, 0.1% (w/v) BSA; pH 7.4) supplemented with 0.45 mg/mL Firefly D-Luciferin free acid. Immediately after agonist addition, luminescence was recorded using a CLARIOstar® Multimode Plate Reader (BMG Labtech, Germany) with no lens (1 sec integration time/well for 1 hour every min). To account for differences in expression/cell density, an average of 6 pre-readings were used to normalise each well's response.

5. NanoBiT BiLC and Venus BiFC assays

To assess GPCR protein:protein interactions with the NanoBiT technology, HEK 293 cells (50,000 cells/well) were seeded in poly-D-lysine coated white clear bottom 96-well plates and reverse transfected (see above) with the plasmids encoding the complementary NanoBiT hemiprotein fragments. For orientation screenings, cells were transfected with two different concentrations (50 and 100 ng/well) of each receptor alone or in combination with the investigated partner (see figure legends) in the presence of empty vector (pcDNA3.1(+)) to normalise the total amount of DNA/well. For studies in the presence of increasing non-tagged receptor competitors, 100 ng of each receptor pair (CB_1R LgBiT + CB_1R SmBiT, 5-$HT_{2A}R$ LgBiT + 5-$HT_{2A}R$ SmBiT and 5-$HT_{2A}R$ LgBiT + CB_1R SmBiT) were co-transfected with

increasing concentrations of the different non-tagged constructs (from 0 to 300 ng/well) and the total amounts of DNA/well were normalised with empty vector (pcDNA3.1(+)). For the screening of stapled peptides, 50 ng/well of both LgBiT CB_1R and SmBiT 5-$HT_{2A}R$ were reverse transfected as previously detailed. 24 hours post-transfection, the cell culture medium was removed and the cells were starved in FBS-free DMEM for 4 h at 37°C in a 5% CO2 humidified atmosphere. The cell culture media was replaced by 100 µL of NanoBiT assay buffer (same as for cAMP measurements) and the plates were pre-equilibrated for 1 hour at RT in the dark. When peptide pre-treatment was required, peptides were added over this pre-equilibration step, unless when studying inhibition kinetics, in which the peptides were administered immediately after the baseline luminescence recording. 25 µL/well of a 5X solution of the Nano-Glo® Live cell reagent containing the cell-permeable furimazine substrate dissolved in Nano-Glo® LCS Dilution buffer were added and the luminescence was immediately monitored in CLARIOstar® Multimode Plate Reader (BMG Labtech, Germany) with no lens (1 sec integration time/well for 1 hour every min).

For BiFC experiments, HEK 293 cells growing at ~80% confluence in 6-well/plates were transfected with Lipofectamine™ 3000 according to manufacturer's instructions with 1.5 µg/well of both Venus YFP complementary plasmids or the corresponding individual receptor constructs. The total amount of DNA/well was kept constant with empty vector (pcDNA3.1(+)). 24 hours post-transfection, the cells were trypsinised according to standard mammalian tissue culture protocols and $5 \cdot 10^5$ viable cells/mL were seeded in poly-D-lysine coated black clear bottom 96-well plates and incubated at 37°C in a 5% CO2 humidified atmosphere O/N. 48 hours post- transfection, the cell culture medium was removed and the cells were starved in FBS-free DMEM for 4 h at 37°C in a 5% CO_2 humidified atmosphere. Prior to fluorescence measurements, the cell culture media was replaced with 100 µL of NanoBiT assay and the plates were pre-equilibrated for 1 hour at RT in the dark. Venus YFP fluorescence was measured at 530 nm (550-50 nm and 517.2 nm dichroic filter) upon excitation (40 flashes/well) at 489 nm (497-15 nm) in a CLARIOstar Multimode Plate Reader (BMG Labtech, Germany) at 25°C.

6. Cell proliferation and toxicity assays

The iCELLigence Real-Time Cell Analyser (RTCA) instrument (Roche Diagnostics GmbH and ACEA Biosciences) was used to analyse cell viability based on changes in electrical impedance over time (defined as cell index; CI). Prior to the experiment, background CI levels of the 8-well E plate (ACEA Biosciences, USA) were measured after the addition of 200 µL/well of pre-warmed complete cell culture medium (see below). Immediately after, 200 µL of the cellular suspension (2.5×10^5 viable HEK 293 cells/mL) were distributed in each well and cellular impedance was continuously monitored (time intervals are indicated in the respective figure) at 37°C in a 5% CO_2 humidified atmosphere. After 24 hours, the E-plates were removed for peptide treatment (4 µM), immediately returned back to the RTCA analyser and CI changes were monitored under the same conditions over the next 48 hours. Normalised cell index (NCI) refers to the ratio between the CI values and CI from the time point immediately prior to ligand addition.

7. Data analysis

Dose-response curves were fitted using a four-parameter logistic nonlinear regression mode. Peptide stability data was fitted using a nonlinear regression mode for dissociation kinetics. All statistical tests, curve fitting and

graphing were performed using GraphPad Prism 8 (GraphPad Software, La Jolla, CA). Information on the statistical test, significance and experimental replicates are provided in the figure legends.

8. Positioning of the staple position

We previously published a model of the CB_1–5-HT_{2A} heterodimer (16). Using this model we identified the amino acids of CB_1R TM5 that would be facing outward from the CB1R receptor and using an i +3 we located the amino acids on which to place the staples using the logic that the staples should be on the opposite side of the helix from the interface of the two receptors.

9. Synthesis of the unnatural amino acid

9.1 General procedure

All experiments were run under an atmosphere of nitrogen, using anhydrous solvents. All chemicals were purchased from Sigma-Aldrich. Analytical thin layer chromatography was performed on Merck Kieselgel 60 F254 plates with visualization by ultraviolet light. Flash chromatography was performed on an Isolera™ Prime (Biotage AB, Sweden). Melting points are uncorrected and were obtained in open capillaries using Electrothermal Melting Point Apparatus. NMR Spectra were recorded on Bruker DPX (^{1}H, 400 MHz; ^{13}C, 100 MHz; ^{19}F, 376 MHz) spectrometers for CDC_l3 solutions. NMR chemical shifts (δ) are given in parts per million (ppm) relative to $CDCl_3$ at 7.26 ppm and coupling constants (*J*) are reported in Hz. Spectral data is reported as follows: chemical shift, integration, multiplicity (s, singlet; d, doublet; t, triplet; m, multiplet). Optical rotations were measured on a JASCO P1010 polarimeter. High resolution mass spectra were recorded at The National Mass Spectrometry Facility & Service at Swansea University Medical School, UK.

*9.2 Synthesis of (S)-1-(2-fluorobenzyl)pyrrolidine-2-carboxylic acid **1***

L-proline (8 g, 69.5 mmol) was added to a solution of freshly ground potassium hydroxide (11.7 g; 3 equiv.) previously dissolved in isopropyl alcohol (90 mL) at 40 °C. As soon as the solution became transparent, 2-fluorobenzyl bromide (8.5 mL) was added dropwise and the solution stirred for 18h at 40 °C. Aqueous hydrochloric acid (37%) was added dropwise to the mixture until the solution reached pH 5-6, as determined using pH indicator strips. The suspension was then cooled in an ice bath for 15 min, filtered and the precipitate thoroughly washed with isopropyl alcohol. All filtrates were combined and concentrated *in vacuo* to give (*S*)-1-(2-fluorobenzyl)pyrrolidine-2-carboxylic acid **1** as a pale orange sticky compound (13.29 g, 93%). For analytical purposes, a small amount of BP was washed with acetone and concentrated *in vacuo* to afford a yellow solid powder of **1**. m.p: 79-81 °C; $[\alpha]D_{20}$ -23.9 (c 0.1 in MeOH); ^{1}H NMR (400 MHz, $CDCl_3$) δ 7.95 (1H, br s, OH), 7.42 (1H, d, J = 6.72 Hz, Ar–C*H*), 7.29-7.24 (1H, m, Ar–C*H*), 7.09 (1H, appt, J = 7.48 Hz, Ar–C*H*), 7.03 (1H, m, Ar–C*H*), 4.25 (1H, d, J = 13.04 Hz, N–CH_2), 3.86 (1H, d, J = 13.05 Hz, N–CH_2), 3.74 (1H, dd, J = 7.83, 6.3 Hz α-C*H*), 3.29 (1H, m, δ-CH_2), 2.49 (1H, dd, J = 9.15, 17.85 Hz, δ-CH_2), 2.21–2.01 (2H, m, β-CH_2), 1.89–1.72 (2H, m, γ-CH_2). ^{13}C NMR (100 MHz; $CDCl_3$) δ 175.41, 162.61, 132.76, 130.19, 124.36, 121.9, 115.9, 67.75, 52.83, 50.84, 29.12, 22.62. Additional peaks arise from rotamers at 130.11, 121.8 and 115.4; ^{19}F NMR (376 MHz; $CDCl_3$) −116.99; HRMS-ESI calculated for $C_{12}H_{15}NO_2F$ $[M + H]^+$ 224.1087, found 224.1081.

*9.3 Synthesis of (S)-N-(2-benzoylphenyl)-1-(2-fluorobenzyl)pyrrolidine-2-carboxamide **2***

(*S*)-1-(2-fluorobenzyl)pyrrolidine-2-carboxylic acid **1** (3.3 g, 14.73 mmol) was dissolved in CH_2Cl_2 (35 mL) at 0 °C. Methanesulfonyl chloride (5 mL, 14.73 mmol) and *N*-methylimidazole (2.6 mL, 32.4 mL) was added in a dropwise manner. After 5 minutes, 2-

aminobenzophenone (2.62 g, 13.3 mol) was added, the ice bath removed, and the reaction mixture heated to 50 °C for 14h. Saturated aqueous sodium hydrogen carbonate solution (30 mL) was added. The two layers were separated, and the aqueous layer extracted with CH_2Cl_2 (3x 30 mL). The organic extracts were combined, dried over sodium sulphate, filtered and concentrated *in vacuo*. Purification by flash column chromatography (SiO_2 eluted with 15% ethyl acetate-hexane) gave the title compound **2** as a pale-yellow powder (2.94 g, 49.4%). m.p: 89-91 °C; $[\alpha]_D^{20}$ -124.1 (c 0.25 in MeOH); ^{1}H NMR (400 MHz, $CDCl_3$) δ 11.43 (1H, s, NH), 8.56 (1H, dd, *J* = 8.19, 1.0 Hz, Ar–C*H*), 7.78–7.76 (2H, m, Ar–C*H*), 7.62 (1H, td, *J* = 7.41, 1.1 Hz), 7.55–7.48 (5H, m, Ar–C*H*), 7.11 (2H, m, Ar–C*H*), 6.94 (1H, td, *J* = 7.51, 1.2 Hz, Ar–C*H*), 6.80 (1H, dt, *J* = 9.22, 1.2 Hz, Ar–C*H*), 3.91 (1H, d, *J* = 13.52 Hz, N–CH_2), 3.74 (1H, dd, *J* = 12.97, 1.2 Hz, N–CH_2), 3.36 (1H, dd, *J* = 10.18, 4.46 Hz, α-C*H*), 3.24 (1H, m, β-CH_2), 2.48 (1H, dd, *J* = 9.08, 16.54 Hz, β-C*H*2), 2.26 (1H, m, δ-CH_2), 1.96 (1H, d, *J* = 3.66, δ-CH_2), 1.89–1.74 (2H, m, γ-CH_2).; ^{13}C NMR (100 MHz; $CDCl_3$) δ 198.1, 174.65, 160.02, 139.19, 138.8, 133.5, 132.7, 131.9, 130.3, 129.11, 129.03, 128.45, 125.8, 125.17, 125.02, 124.08, 122.5, 121.7, 115.42, 115.2, 68.11, 53.94, 52.2, 31.27, 24.45; ^{19}F NMR (376 MHz; $CDCl_3$) −117.6; HRMS-ESI (calculated for $C_{25}H_{24}N_2O_2F$ $[M + H]^+$ 403.1822, found 403.1816

*9.4 Synthesis of Ni-Ala-FBPB **3***

(*S*)-N-(2-Benzoylphenyl)-1-(2-fluorobenzyl)pyrrolidine-2-carboxamide **2** (2.0 g, 4.96 mmol) was dissolved in methanol (55 mL) at 50 °C. $Ni(NO_3)_2{\cdot}6H_2O$ (2.9 g, 9.93 mmol) and L-alanine (0.89 g, 9.93 mmol) were added to the reaction mixture and after 3 minutes, freshly ground potassium hydroxide (1.95 g, 34.57 mmol) was added and the mixture was heated to 70 °C for 1.5h.The reaction mixture was cooled on the room temperature and concentrated. The residue was taken up in distilled water (50 mL) and extracted with EtOAc (3 x 50 mL). The combined organic layers were washed with brine solution (3 x 150 mL), dried over sodium sulphate, filtrated, concentrated *in vacuo* and extensively washed with $CHCl_3$ to give the title compound **3** as a red crystalline solid (2.61 g, 99%). m.p: 279–281 °C (lit[1]: 283–285 °C); $[\alpha]_D^{20}$ +3432.9 (*c* 0.05 in $CHCl_3$) (lit[1]: +3126.6 (*c* 0.05 in $CHCl_3$); ^{1}H NMR (400 MHz, $CDCl_3$) δ 8.30 (1H, td, *J* = 7.52, 1.72 Hz, Ar–C*H*), 8.11 (1H, d, *J* = 8.52 Hz, Ar–C*H*), 7.53–7.49 (2H m, Ar–C*H*), 7.45 (1H, d, *J* = 7.46, Ar–C*H*), 7.24–7.20 (2H, m, Ar–C*H*), 7.19–7.12 (2H, m, Ar–C*H*), 7.05 (1H, appt, *J* = 9.49 Hz, Ar–C*H*), 6.95 (1H, d, *J* = 7.39, Ar–C*H*), 6.69–6.62 (2H, m, Ar–C*H*), 4.40 (1H, d, *J* = 13.06, N–C*H*H), 3.90 (1H, q, *J* = 7.01 Hz, α-C(Me)*H*), 3.82 (1H, d, *J* = 13.0Hz, N–CH*H*), 3.69 (1H, d, *J* = 6.71, β(Pro)-C*H*H), 3.51–3.46 (2H, m, α(Pro)-C*H*, γ(Pro)-CH*H*), 2.81 (1H, m, *δ*(Pro)-C*H*H), 2.56 (1H, m, *δ*(Pro)-CH*H*), 2.21 (1H, dt, *J* = 12.65, 6.50 Hz, γ(Pro)-CH*H*), 2.05 (1H, td, *J* = 11.59, 6.03 Hz, β(Pro)-CH*H*), 1.58 (3H, d, *J* = 7.03 Hz, CH_3); ^{13}C NMR (100 MHz, $CDCl_3$) δ 180.49, 180.1, 170.35, 142.06, 134.21, 133.47, 133.2, 132.18, 131.29, 128.9, 127.5, 127.23, 126.62, 124.55, 123.92, 120.87, 120.87, 120.33, 120.30, 116.24, 116.02, 70.33, 66.64, 57.07, 55.6, 30.7, 24.16, 21.84; ^{19}F NMR (376 MHz, $CDCl_3$) δ −112.66; HRMS-ASAP calculated for $C_{28}H_{27}N_3O_3FNi$ $[M + H^+]$ 532.1381, found 530.1357

*9.5 Synthesis of S5-Ni-Ala-FBFB **4***

Finely ground sodium hydroxide (0.31 g, 7.52 mmol) was added to DMF (15 mL) under a nitrogen atmosphere with stirring at 5 °C. Ni-Ala-FBPB **3** (1 g, 1.88 mmol) was added and the reaction mixture stirred for 5 min. After the solution darkened in colour, the ice bath was removed and solution of 1-bromo-4-pentene (0.873 g, 5.64 mmol) was added to the reaction mixture. The reaction mixture was heated to 50 °C and left to stir for 1h. Upon completion of the reaction, the mixture was quenched with distilled water (10 mL). The mixture was concentrated *in vacuo*, taken up in distilled water (15 mL) and extracted with CH_2Cl_2 (3 x 20 mL). The combined organic extracts were washed with aqueous lithium chloride solution

(5%, 3 x 40 mL) to thoroughly remove any DMF residue followed by brine (3 x 40 mL). The mixture was then dried over sodium sulfate and concentrated *in vacuo*. Purification by flash column chromatography (EtOAc-hexane=1:1) gave the title compound **4** as a deep red-orange solid (0.69 g, 61%). m.p: 196-198 °C (lit[2]:190–192 °C) $[\alpha]_D^{20}$ +2201.1 (c 0.05, $CHCl_3$) (lit[2]:+2271.2 (c 0.05, $CHCl_3$); ^{1}H NMR (400 MHz, $CDCl_3$) δ 8.29 (1H, td, *J* = 7.4, 1.0 Hz, Ar–CH), 8.03 (1H, d, *J* = 8.5 Hz, Ar–C*H*), 7.51–7.44 (2H, m, Ar–C*H*), 7.38 (1H, m, Ar–C*H*), 7.33 (1H, m, Ar–C*H*), 7.29 (1H, m Ar–C*H*), 7.20 (1H, appt, *J* = 7.4 Hz, Ar–C*H*), 7.16 (1H, ddd, *J* = 8.4, 6.2, 2.2 Hz, Ar–C*H*), 7.06 (1H, appt, *J* = 9.1 Hz, Ar–C*H*), 6.97 (1H, d, *J* = 7.6 Hz, Ar–C*H*), 6.68–6.61 (2H, m, Ar–C*H*), 5.86 (1H, ddt, *J* = 17.0, 10.3, 6.5 Hz, C*H*CH_2), 5.08 (1H, dd, *J* = 17.0, 1.0 Hz, CHCH_2*cis*), 5.02 (1H, d, *J* = 10.3 Hz, CHCH_2*trans*), 4.52 (1H, d, *J* = 13.1 Hz, N–C*H*H), 3.95 (1H, d, *J* = 13.1 Hz, N–CH*H*), 3.60 (1H, dd, *J* = 9.9, 6.5 Hz, α(Pro)-C*H*), 3.41 (1H, dd, *J* = 10.7, 6.4 Hz, *δ*(Pro)-C*H*H), 3.26 (1H, m, β(Pro)-C*H*H), 2.78 (1H, m, γ(Pro)-C*H*H), 2.52 (1H, m, γ(Pro)-CH*H*), 2.40 (1H, m, γ-C*H*H), 2.17–1.98 (5H, m, δ-C*H*2, γ-CH*H*, *δ*(Pro)-CH*H*, β(Pro)-CH*H*), 1.75–1.62 (2H, m, β-CH_2), 1.23 (3H, s, CH_3); ^{13}C NMR (101 MHz, $CDCl_3$) *δ* 182.38, 180.15, 172.4, 141.5, 137.83, 136.44, 134.2, 133.45, 131.62, 131.31, 130.32, 129.41, 128.77, 127.97, 127.34, 126.94, 124.51, 124.0, 120.8, 120.33, 116.28, 116.0, 115.44, 78.1, 70.15, 56.67, 55.86, 39.78, 33.71, 30.54, 29.6, 25.27, 23.25; ^{19}F NMR (376 MHz, $CDCl_3$) *δ* −113.7; HRMS-ESI calculated for $C_{33}H_{35}N_3O_3FNi$ $[M+H]^+$ 598.2016, found 598.6649.

*9.6 Synthesis of S-pentenylalanine **5***

3M hydrochloric acid (3.1 mL, 24 equivalent) was warmed to 70°C. A solution of S5-Ni-Ala-FBFB **4** (300 mg) dissolved in methanol (25 mL) was added drop wise to pre-warmed HCl. In 5 min, a colour change from red to transparent green/yellow was observed. The mixture was left stirring for an additional 20 min and then cooled to room temperature. After removing the methanol *in vacuo,* the residue was taken up in water (20 mL) and extracted with DCM (3 x 20 mL). The organic extracts were combined, dried ($MgSO_4$) and concentrated *in vacuo* to reclaim **2**. A few drops of 1M NaOH were added to the green aqueous solution to precipitate Ni-salts. After 2 min centrifugation at 600 rpm, the filtrate was decanted and after removal of the water in vacuo, *S*-pentenylalanine **5** was isolated as a white powder (70 mg, 89%). m.p: 242-244°C (lit[2]: 250–252 °C) $[\alpha]_D^{20}$ +3.09 (c 0.05, MeOH) (lit[2]: +3.22 (c 0.05, MeOH, 25°C)); ^{1}H NMR (400 MHz, D_2O) δ 5.74 (1 H, dd, *J* = 10.23, 17.08 Hz, $CHCH_2$), 4.94 (2 H, m, $CHCH_2$), 1.99 (2 H, d, *J* = 6.55 Hz, δ-CH_2), 1.85 (1 H, m, β-CHH), 1.74 (1 H, m, β-CHH), 1.50–1.35 (4 H, m, CH_3, γ-CHH), 1.26 (1 H, m, γ-CHH); ^{13}C NMR (100 MHz, D_2O) δ 177.0, 138.7, 115, 61.6, 36.7, 32.8 , 22.5, 22.5; HRMS-ESI (calculated for $C_8H_{16}NO_2$ $[M+H^+]$ 158.1181, found 158.1562.

*9.7 Fmoc-S-pentenylalanine **6***

Potassium carbonate (70 mg, 0.51 mmol) and *S*-pentenylalanine **5** (40 mg, 0.25 mmol) was dissolved in water (1 mL) and cooled to 0 °C. pH was routinely checked with the pH indicators and after confirming the basic conditions, Fmoc-Cl (100 mg, 0.38 mmol) was dissolved in dioxane (1.4 mL) and added to the reaction mixture over 10 min. The reaction was then warmed to the room temperature and stirred for 36h. An excess volume of water was added and the mixture extracted with ethyl acetate (2 x 10 mL). The combined organic phases were then extracted with saturated bicarbonate solution (2 x 20 mL) and the aqueous layer acidified to pH 1 with 6M HCl. The combined aqueous phases were then extracted with EtOAc (3 x 20 mL). The organic phases were combined, dried ($MgSO_4$) and concentrated *in vacuo.* Purification by column chromatography (SiO_2 eluted with MeOH:CH_2Cl_2:AcOH (97:2:1) gave Fmoc-*S*-pentenylalanine **6** as a white powder (35mg, 21%). m.p: 225-227 °C $[\alpha]^D_{20}$ +3.6 (c 1.0, MeOH) (lit[2]: +3.5 (c 1.0, MeOH, 25°C); ^{1}H NMR (400 MHz, $CDCl_3$) δ 7.77 (dd, *J* = 7.3, 3.7

Hz, 2H), 7.59 (s, 2H), 7.45 – 7.38 (m, 2H), 7.35 – 7.28 (m, 2H), 5.75 (s, 1H), 5.46 (s, 1H), 4.99 (t, J = 14.2 Hz, 2H), 4.42 (s, 2H), 4.22 (s, 1H), 2.05 (s, 2H), 1.86 (s, 1H), 1.60 (s, 3H), 1.27 (s, 2H). ^{13}C NMR (101 MHz, $CDCl_3$) δ 179.18, 154.82, 143.81, 141.37, 138.02, 127.72, 127.09, 125.02, 120.01, 115.10, 66.56, 59.76, 47.23, 36.22, 33.39, 23.29; HRMS-ESI (calculated for $C_{23}H_{26}NO_4$ [M+H$^+$] 380.1862, found 380.1860.

10. Synthesis and purification of the TM Peptides

Transmembrane (TM) peptides were synthesized on a fully automated Syro I (Biotage AB, Sweden) instrument using standard procedures for Fmoc-solid phase peptide synthesis on a 100 mg preloaded H-Arg(Pbf)-HMPB NovaPEG or H-Phe-HMPB NovaPEG resin (Merck Millipore, Darmstadt, Germany) with the resin loading of 0.48 mmol/g or 0.63 mmol/g, respectively, as a solid support. The preloaded arginine resin was swollen in DMF for 20 minutes and checked for potential clumping since clumped resin may impact the synthesis. After the swelling, coupling was achieved using 4 equivalents of the following: Fmoc-protected amino acid, HOBt and HBTU and 8 equivalents of DIPEA in NMP. Each coupling reaction was left for 45 minutes and performed twice to ensure complete coupling. Fmoc deprotection was achieved using 40% piperidine in DMF (3 x 1.5 mL). After final incorporation of the last amino acid, the Fmoc group was removed and the resin was washed thoroughly with DMF, DCM and 1:1 DCM:MeOH to remove any residual DMF and dried *in vacuo*. Cleavage from the solid support was carried out using TFA/water/EDT/TIPS (v/v/v/v = 94/2.5/2.5/1, 10 mL/0.1 g resin) in case of TM5-7 for 3h. For peptides **7-11** TFA/water/TIPS (v/v/v = 95/2.5/2.5, 10 mL/0.1 g resin) was used. The resin was washed with TFA (10 mL), combined with the cleavage cocktail and concentrated *in vacuo*. The crude peptide was precipitated with a 10-fold excess of cooled (-20°C) diethyl ether leaving a white precipitate.

Following crude peptide isolation, the peptides were dissolved in methanol (40 mL), filtered and purified by preparative RP-HPLC (Agilent 1200 Infinity) using an Aeris PEPTIDE 5µm XB-C18 column, 150 x 21.2 mm with a gradient of 95:5 water:MeOH with 0.05% TFA to 5:95 water:MeOH over 15 min returning to 95:5 water:MeOH over 5 min at a flow rate of 20mL/min at the detection wavelength of 214 nm. Analytical RP-HPLC was then used to assess the purity of the products after the purification and was performed on an Agilent 1200 using an Aeris Peptide 5µm XB-C18 column, 150 x 4.6 mm with the same conditions as above. Following purification, the peptides were concentrated, resuspended in distilled water and lyophilized. Mass analysis was performed to determine the identities of TM peptides by MALDI-TOF mass spectrometry, using sinapinic acid as the ionization matrix.

11. Synthesis and purification of the stapled peptides

Peptides were synthesized on a Syro I fully automated peptide synthesizer using Rink amide LL 100-200 mesh resin (0.36 mmol⁄g), at 36 µmol scale as described above. Coupling frequency and incubation times were 2 × 45 min for standard amino acid residues, 2 × 60 min for the olefinic non-natural amino acid **6**, and 2 × 60 min for the residue following a non-natural amino acid. After the automated synthesis, the ring-closing metathesis was performed on the peptide while still on the solid support in a disposable fritted reaction vessel. The peptide resin was cyclized in the presence of Grubbs catalyst second-generation catalyst (10 mM) in anhydrous 1,2-dichloroethane (DCE) for 4h at room temperature. Completeness of the ring-closing metathesis (RCM) reaction was monitored by HPLC. The resin- bound peptide was washed with DCE and then with DCM, DCM:MeOH (1:1) and dried under vacuum. The Fmoc group was removed with 30% piperidine in DMF (2 x 10 min), washed with DMF, DCM, DCM:MeOH (1:1) and dried under vacuum. The

stapled peptides were cleaved from the solid support by treatment with TFA:H_2O:TIPS (95/2.5/2.5) for 2-3h at room temperature. The resin was washed with TFA (10 mL), combined with the cleavage cocktail and concentrated *in vacuo*. The crude peptide was precipitated with a 10-fold excess of cooled (-20°C) diethyl ether leaving a white precipitate. Purification, HPLC and MALDI-TOF analysis were performed as above.

12. Monitoring the RCM reaction

An analytical test for monitoring the progress of the RCM reaction was performed in a similar manner as described by Young Woo et al.(24) A 50 µL aliquot of resin suspension was taken out of the reaction and washed with 200 µL of anhydrous DCE under nitrogen bubbling. After that initial wash, the reaction solution was washed with DCM and DCM:MeOH (1:1), cleaved with 60 µL cleavage cocktail (TFA:H20:TIS (95/2.5/2.5) for 40 min, resin removed, TFA evaporated and the peptide precipitated with cold diethyl ether. The pellet was left to air dry before dissolving it in 25 µL of 95:5 water:MeOH with 0.05% TFA and analysed using analytical RP-HPLC.

13. CD helicity measurements

CD spectra were recorded on a Jasco J-810 with a total of three scans from 195 to 260 nm in 0.5 nm increments. The averaged scans were collected at the scanning speed of 200 nm/min using a 1-mm path length cell. Peptides were prepared as described in Greenfield's protocol(41), dissolved in MilliQ deionized water with the target concentration between 30 to 50 µM with the exact concentration then confirmed using a BCA Protein Assay Kit according to the manufacture's protocol. The CD Spectrum of the MilliQ Water was subtracted from the spectrum of the sample.

The Jasco J-810 generates the raw output in ellipticity and is measured in millidegrees (mdeg). This was first converted to ***molar ellipticity [θ]*** with units of $\frac{d \quad \times c^{\ 2}}{d}$. Once the precise concentration was confirmed, the molar ellipticity [θ] was calculated as:

$$[\theta] = \frac{\theta_o \quad \times 10^6}{c \times l \times n}$$

Where ***c*** is the sample concentration (µM), ***l*** is the path length (mm), ***n*** is the number of peptides bonds (calculated as amino acid residues – 1) and $\boldsymbol{\theta_{obs}}$ is the observed ellipticity (mdeg). To calculate the % of helicity, the ***mean residue ellipticity [MRW]*** and $\boldsymbol{\theta_{MAX}}$ were calculated according to Forood et al.(42) and others:(43–45)

where $\boldsymbol{\theta_{222}}$ is molar ellipticity at 222nm, ***c*** is molar concentration of the peptide and ***n*** is a number of amino acids residues.

$$[\theta]_m \quad = (-44000 + 250T) \times (1 - \frac{k}{n})$$

where ***T*** is the temperature (273 K) and ***k*** the number of non-hydrogen-bonded peptide carbonyl. According to Shepherd et al. (44), intramolecular hydrogen bonds are characteristic of alpha helicity so inclusion/exclusion of N-terminal acetyl group or C-terminal amide group effects k. For Ac-[Peptide]-NH_2 k=3; H-[Peptide]-NH_2 k=2 and for H-[Peptide]-OH k=1.

Percent helicity was then calculated as:

$$\%\, he \quad = \frac{[\theta]_2}{[\theta]_m} \times 100$$

14. Proteolytic Stability Studies

Stability against trypsin: To a 100 µL of peptide solution (100 µM, dissolved in ammonium bicarbonate buffer, pH 7.5), 60 µL ammonium bicarbonate buffer (pH 7.5) was added, together with temperature-equilibrated (37± 1 C) 20 µL trypsin (5 µg/mL) from porcine pancreas (Sigma, 13,000-20,000 BAEE units/mg protein). Peptides were incubated for 15, 30, 60, 120, 240

and 480 min and then MeOH (HPLC Grade) + 0.05% TFA was added. The samples were then centrifuged (15,000 rpm) and the supernatant analyzed, using Fmoc-Gly (10 µL, 0.2 mM) as an internal standard. The digestion at each time points was repeated three times to give the average values along with standard deviations. The amount of intact peptide remained in the mixture was quantified by RP-HPLC. The experiment was repeated twice on different days.

Stability against chymotrypsin: To a 100 µL of peptide solution (100 µM, dissolved in ammonium bicarbonate buffer, pH 7.5), 60 µL ammonium bicarbonate buffer (pH 7.5) was added, together with temperature-equilibrated (37± 1 C) 20 µL α-chymotrypsin (5 µg/mL) from bovine pancreas (Sigma, Type II, activity > 40 units/mg protein). Peptides were incubated for 15, 30, 60, 120, 240 and 480 min and then MeOH (HPLC Grade) + 0.05% TFA was added. The samples were then centrifuged (15,000 rpm) and supernatant analyzed in a similar manner as described above. The experiment was repeated twice on different days.

Stability in the mouse serum: To 200 µL of fresh non-sterile mouse serum was added 25 µL of peptide solution (100 µM, dissolved in ammonium bicarbonate buffer, pH 7.5, containing 10% DMSO), and the mixture was incubated at 37 ºC. At the specified time, an aliquot of incubation mixture was withdrawn and quenched by addition of equal volume of 15% trichloroacetic acid in acetonitrile to precipitate out serum proteins over ice for 30 min. The mixture was then centrifuged at 13,500 rpm for 10 min, and the supernatant was collected and analyzed by HPLC in a similar manner as described previously. The experiment was repeated twice on different days.

Acknowledgments: We acknowledge the EPSRC UK National Mass Spectrometry Facility at Swansea University.

Conflict of interest: The authors declare that they have no conflicts of interest with the contents of this article.

References

1. Choe, H.-W., Kim, Y. J., Park, J. H., Morizumi, T., Pai, E. F., Krauss, N., Hofmann, K. P., Scheerer, P., and Ernst, O. P. (2011) Crystal structure of metarhodopsin II. *Nature*. **471**, 651–5
2. Huang, J., Chen, S., Zhang, J. J., and Huang, X.-Y. (2013) Crystal structure of oligomeric β1-adrenergic G protein-coupled receptors in ligand-free basal state. *Nat. Struct. Mol. Biol.* **20**, 419–425
3. Manglik, A., Kruse, A. C., Kobilka, T. S., Thian, F. S., Mathiesen, J. M., Sunahara, R. K., Pardo, L., Weis, W. I., Kobilka, B. K., and Granier, S. (2012) Crystal structure of the μ-opioid receptor bound to a morphinan antagonist. *Nature*. **485**, 321–326
4. Salom, D., Lodowski, D. T., Stenkamp, R. E., Trong, I. L., Golczak, M., Jastrzebska, B., Harris, T., Ballesteros, J. A., and Palczewski, K. (2006) Crystal structure of a photoactivated deprotonated intermediate of rhodopsin. *Proc. Natl. Acad. Sci.* **103**, 16123–16128
5. Scheerer, P., Park, J. H., Hildebrand, P. W., Kim, Y. J., Krauss, N., Choe, H.-W., Hofmann, K. P., and Ernst, O. P. (2008) Crystal structure of opsin in its G-protein-interacting conformation. *Nature*. **455**, 497–502
6. Zhang, C., Srinivasan, Y., Arlow, D. H., Fung, J. J., Palmer, D., Zheng, Y., Green, H. F., Pandey, A., Dror, R. O., Shaw, D. E., Weis, W. I., Coughlin, S. R., and Kobilka, B. K. (2012) High-resolution crystal structure of human protease-activated receptor 1. *Nature*. **492**, 387–392
7. Murakami, M., and Kouyama, T. (2008) Crystal structure of squid rhodopsin. *Nature*. **453**, 363–367
8. Wu, B., Chien, E. Y. T., Mol, C. D., Fenalti, G., Liu, W., Katritch, V., Abagyan, R., Brooun, A., Wells, P., Bi, F. C., Hamel, D. J., Kuhn, P., Handel, T. M., Cherezov, V., and Stevens, R. C. (2010) Structures of the CXCR4 Chemokine GPCR with Small-Molecule and Cyclic Peptide Antagonists. *Science*. 10.1126/science.1194396
9. Busnelli, M., Kleinau, G., Muttenthaler, M., Stoev, S., Manning, M., Bibic, L., Howell, L. A., McCormick, P. J., Di Lascio, S., Braida, D., Sala, M., Rovati, G. E., Bellini, T., and Chini, B. (2016) Design and Characterization of Superpotent Bivalent Ligands Targeting Oxytocin Receptor Dimers via a Channel-Like Structure. *J. Med. Chem.* **59**, 7152–7166
10. Cai, X., Bai, B., Zhang, R., Wang, C., and Chen, J. (2017) Apelin receptor homodimer-oligomers revealed by single-molecule imaging and novel G protein-dependent signaling. *Sci. Rep.* **7**, 40335–40335
11. Hebert, T. E., Moffett, S., Morello, J.-P., Loisel, T. P., Bichet, D. G., Barret, C., and Bouvier, M. (1996) A Peptide Derived from a β2-Adrenergic Receptor Transmembrane Domain Inhibits Both Receptor Dimerization and Activation. *J. Biol. Chem.* **271**, 16384–16392
12. Wang, J., He, L., Combs, C. A., Roderiquez, G., and Norcross, M. A. (2006) Dimerization of CXCR4 in living malignant cells: control of cell migration by a synthetic peptide that reduces homologous CXCR4 interactions. *Mol. Cancer Ther.* **5**, 2474–2483
13. Lee, L. T. O., Ng, S. Y. L., Chu, J. Y. S., Sekar, R., Harikumar, K. G., Miller, L. J., and Chow, B. K. C. (2014) Transmembrane peptides as unique tools to demonstrate the in vivo action of a cross-class GPCR heterocomplex. *FASEB J.* 10.1096/fj.13-246868
14. Borroto-Escuela, D. O., Carlsson, J., Ambrogini, P., Narváez, M., Wydra, K., Tarakanov, A. O., Li, X., Millón, C., Ferraro, L., Cuppini, R., Tanganelli, S., Liu, F., Filip, M., Diaz-Cabiale, Z., and

Fuxe, K. (2017) Understanding the Role of GPCR Heteroreceptor Complexes in Modulating the Brain Networks in Health and Disease. *Front. Cell. Neurosci.* 10.3389/fncel.2017.00037

15. Ali, A. M., Atmaj, J., Van Oosterwijk, N., Groves, M. R., and Dömling, A. (2019) Stapled Peptides Inhibitors: A New Window for Target Drug Discovery. *Comput. Struct. Biotechnol. J.* **17**, 263–281
16. Viñals, X., Moreno, E., Lanfumey, L., Cordomí, A., Pastor, A., de La Torre, R., Gasperini, P., Navarro, G., Howell, L. A., Pardo, L., Lluís, C., Canela, E. I., McCormick, P. J., Maldonado, R., and Robledo, P. (2015) Cognitive Impairment Induced by Delta9-tetrahydrocannabinol Occurs through Heteromers between Cannabinoid CB1 and Serotonin 5-HT2A Receptors. *PLoS Biol.* **13**, e1002194
17. Dixon, A. S., Schwinn, M. K., Hall, M. P., Zimmerman, K., Otto, P., Lubben, T. H., Butler, B. L., Binkowski, B. F., Machleidt, T., Kirkland, T. A., Wood, M. G., Eggers, C. T., Encell, L. P., and Wood, K. V. (2016) NanoLuc Complementation Reporter Optimized for Accurate Measurement of Protein Interactions in Cells. *ACS Chem. Biol.* **11**, 400–408
18. Alexander, S. P., Christopoulos, A., Davenport, A. P., Kelly, E., Marrion, N. V., Peters, J. A., Faccenda, E., Harding, S. D., Pawson, A. J., Sharman, J. L., Southan, C., and Davies, J. A. (2017) THE CONCISE GUIDE TO PHARMACOLOGY 2017/18: G protein-coupled receptors. *Br. J. Pharmacol.* **174**, S17–S129
19. Qin, J. Y., Zhang, L., Clift, K. L., Hulur, I., Xiang, A. P., Ren, B.-Z., and Lahn, B. T. (2010) Systematic Comparison of Constitutive Promoters and the Doxycycline-Inducible Promoter. *PLoS ONE*. **5**, e10611–e10611
20. Vidi, P.-A., Chemel, B. R., Hu, C.-D., and Watts, V. J. (2008) Ligand-dependent oligomerization of dopamine D(2) and adenosine A(2A) receptors in living neuronal cells. *Mol. Pharmacol.* **74**, 544–51
21. Kilpatrick, L. E., Humphrys, L. J., and Holliday, N. D. (2015) A G protein-coupled receptor dimer imaging assay reveals selectively modified pharmacology of neuropeptide Y Y1/Y5 receptor heterodimers. *Mol. Pharmacol.* **87**, 718–32
22. Ciruela, F., Vilardaga, J.-P., and Fernández-Dueñas, V. (2010) Lighting up multiprotein complexes: lessons from GPCR oligomerization. *Trends Biotechnol.* **28**, 407–415
23. Ziegler, A., Nervi, P., Dürrenberger, M., and Seelig, J. (2005) The Cationic Cell-Penetrating Peptide CPP ^{TAT} Derived from the HIV-1 Protein TAT Is Rapidly Transported into Living Fibroblasts: Optical, Biophysical, and Metabolic Evidence †. *Biochemistry*. **44**, 138–148
24. Kim, Y.-W., Grossmann, T. N., and Verdine, G. L. (2011) Synthesis of all-hydrocarbon stapled α-helical peptides by ring-closing olefin metathesis. *Nat. Protoc.* **6**, 761–771
25. Bird, G. H., Madani, N., Perry, A. F., Princiotto, A. M., Supko, J. G., He, X., Gavathiotis, E., Sodroski, J. G., and Walensky, L. D. (2010) Hydrocarbon double-stapling remedies the proteolytic instability of a lengthy peptide therapeutic. *Proc. Natl. Acad. Sci. U. S. A.* **107**, 14093–8
26. Pelay-Gimeno, M., Glas, A., Koch, O., and Grossmann, T. N. (2015) Structure-Based Design of Inhibitors of Protein-Protein Interactions: Mimicking Peptide Binding Epitopes. *Angew. Chem. Int. Ed.* **54**, 8896–8927
27. Schafmeister, C. E., Po, J., and Verdine, G. L. (2000) An All-Hydrocarbon Cross-Linking System for Enhancing the Helicity and Metabolic Stability of Peptides. *J. Am. Chem. Soc.* **122**, 5891–5892
28. Walensky, L. D., and Bird, G. H. (2014) Hydrocarbon-stapled peptides: principles, practice, and progress. *J. Med. Chem.* **57**, 6275–6288
29. Aillard, B., Robertson, N. S., Baldwin, A. R., Robins, S., and Jamieson, A. G. (2014) Robust asymmetric synthesis of unnatural alkenyl amino acids for conformationally constrained α-helix peptides. *Org. Biomol. Chem.* **12**, 8775–8782
30. Saghyan, A. S., Dadayan, A. S., Dadayan, S. A., Mkrtchyan, A. F., Geolchanyan, A. V., Manasyan, L. L., Ajvazyan, H. R., Khrustalev, V. N., Hambardzumyan, H. H., and Maleev, V. I. (2010) Rapid asymmetric synthesis of amino acids via NiII complexes based on new fluorine containing chiral auxiliaries. *Tetrahedron Asymmetry*. **21**, 2956–2965

31. Brea, J., Castro, M., Giraldo, J., López-Giménez, J. F., Padín, J. F., Quintián, F., Cadavid, M. I., Vilaró, M. T., Mengod, G., Berg, K. A., Clarke, W. P., Vilardaga, J.-P., Milligan, G., and Loza, M. I. (2009) Evidence for distinct antagonist-revealed functional states of 5-hydroxytryptamine(2A) receptor homodimers. *Mol. Pharmacol.* **75**, 1380–91
32. Wager-Miller, J., Westenbroek, R., and Mackie, K. (2002) Dimerization of G protein-coupled receptors: CB1 cannabinoid receptors as an example. *Chem. Phys. Lipids*. **121**, 83–9
33. Szidonya, L., Cserzo, M., and Hunyady, L. (2008) Dimerization and oligomerization of G-protein-coupled receptors: debated structures with established and emerging functions. *J. Endocrinol.* **196**, 435–53
34. Cottet, M., Faklaris, O., Zwier, J. M., Trinquet, E., Pin, J.-P., and Durroux, T. (2011) Original Fluorescent Ligand-Based Assays Open New Perspectives in G-Protein Coupled Receptor Drug Screening. *Pharmaceuticals*. **4**, 202–214
35. Kroeze, W. K., Sassano, M. F., Huang, X.-P., Lansu, K., McCorvy, J. D., Giguère, P. M., Sciaky, N., and Roth, B. L. (2015) PRESTO-Tango as an open-source resource for interrogation of the druggable human GPCRome. *Nat. Struct. Mol. Biol.* **22**, 362–369
36. Kim, M. W., Wang, W., Sanchez, M. I., Coukos, R., von Zastrow, M., and Ting, A. Y. (2017) Time-gated detection of protein-protein interactions with transcriptional readout. *eLife*. **6**, e30233
37. Yano, H., Cai, N. S., Javitch, J. A., and Ferré, S. (2018) Luciferase complementation based-detection of G-protein-coupled receptor activity. *BioTechniques*. **65**, 9–14
38. Moreno, E., Chiarlone, A., Medrano, M., Puigdellívol, M., Bibic, L., Howell, L. A., Resel, E., Puente, N., Casarejos, M. J., Perucho, J., Botta, J., Suelves, N., Ciruela, F., Ginés, S., Galve-Roperh, I., Casadó, V., Grandes, P., Lutz, B., Monory, K., Canela, E. I., Lluís, C., McCormick, P. J., and Guzmán, M. (2018) Singular Location and Signaling Profile of Adenosine A2A-Cannabinoid CB1 Receptor Heteromers in the Dorsal Striatum. *Neuropsychopharmacology*. **43**, 964–977
39. Borroto-Escuela, D. O., Craenenbroeck, K. V., Romero-Fernandez, W., Guidolin, D., Woods, A. S., Rivera, A., Haegeman, G., Agnati, L. F., Tarakanov, A. O., and Fuxe, K. (2011) Dopamine D2 and D4 receptor heteromerization and its allosteric receptor–receptor interactions. *Biochem. Biophys. Res. Commun.* **404**, 928–934
40. González-Vera, J. A., Medina, R. A., Martín-Fontecha, M., Gonzalez, A., de la Fuente, T., Vázquez-Villa, H., García-Cárceles, J., Botta, J., McCormick, P. J., Benhamú, B., Pardo, L., and López-Rodríguez, M. L. (2017) A new serotonin 5-HT6 receptor antagonist with procognitive activity - Importance of a halogen bond interaction to stabilize the binding. *Sci. Rep.* **7**, 41293
41. Greenfield, N. J. (2006) Using circular dichroism spectra to estimate protein secondary structure. *Nat. Protoc.* **1**, 2876–2890
42. Forood, B., Feliciano, E. J., and Nambiar, K. P. (1993) Stabilization of alpha-helical structures in short peptides via end capping. *Proc. Natl. Acad. Sci. U. S. A.* **90**, 838–842
43. Wang, D., Chen, K., Kulp, J. L., and Arora, P. S. (2006) Evaluation of Biologically Relevant Short α-Helices Stabilized by a Main-Chain Hydrogen-Bond Surrogate. *J. Am. Chem. Soc.* **128**, 9248–9256
44. Shepherd, N. E., Hoang, H. N., Abbenante, G., and Fairlie, D. P. (2005) Single turn peptide alpha helices with exceptional stability in water. *J. Am. Chem. Soc.* **127**, 2974–2983
45. Kawamoto, S. A., Coleska, A., Ran, X., Yi, H., Yang, C.-Y., and Wang, S. (2012) Design of Triazole-stapled BCL9 α-Helical Peptides to Target the β-Catenin/B-cell CLL/lymphoma 9 (BCL9) Protein-Protein Interaction. *J. Med. Chem.* **55**, 1137–1146

FOOTNOTES

Funding was provided by the University of East Anglia through studentships for JB and a BBSRC DTP to PJM and LAH for LB as well as start-up funds from QMUL.

The abbreviations used are: GPCR, G-protein coupled receptor, TM, transmembrane domain, CB_1R, cannabinoid receptor 1, 5-HT_{2A}, serotonin receptor type 2A

Peptide	Amino Acid Sequence
CB_1R TM5	ETYLMFWIGVTSVLLLFIVYAYMYILW GRKKRRQRRR
CB_1R TM5a	VLLLFIVYAYMYILW
CB_1R TM5b	VLLLFIVYAYMYILW
CB_1R TM5c	VYAYMYILW
CB_1R TM5d	VYAYMYILW

Table 1: Potential sites within the CB_1R TM5 peptide amino acid sequence to introduce the hydrocarbon staple were identified based on a previously published molecular model (see Methods). The positions (facing the lipids) to build the stapled peptides (at i and i+3/4) are shown in red. The TAT amino acid sequence is shown in orange.

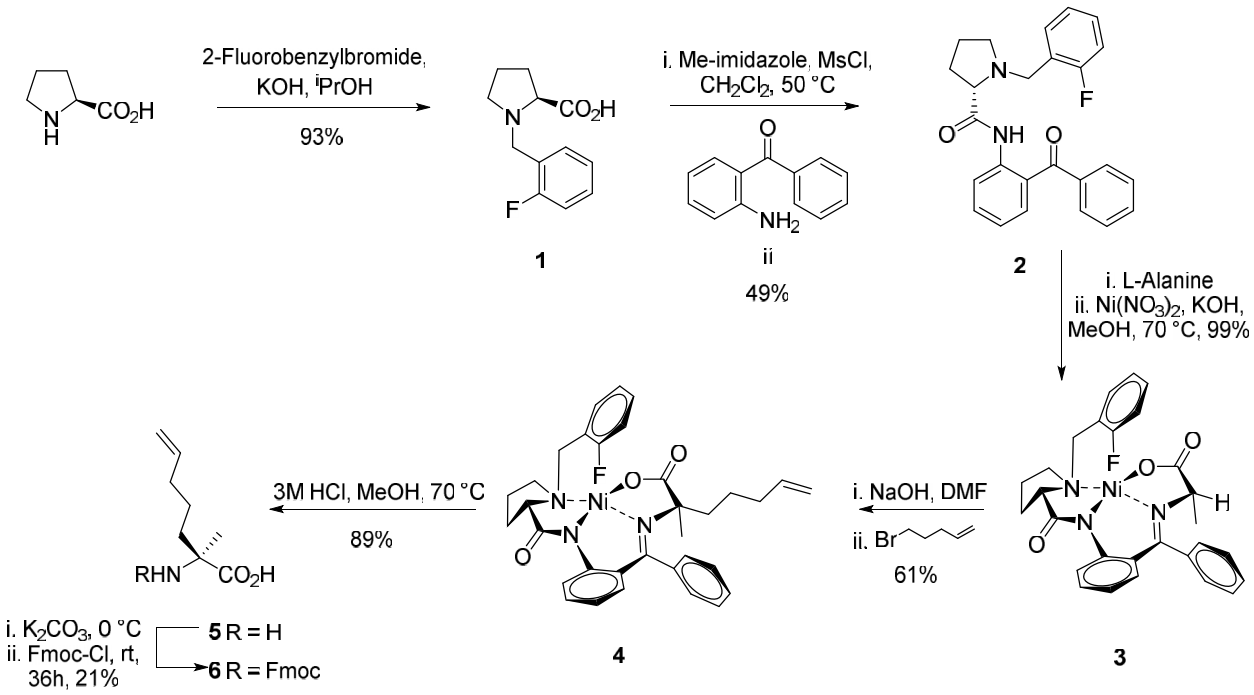

Scheme 1: Synthesis of the Fmoc protected unnatural amino acid S-pentenylalanine (Fmoc-S_5-OH).

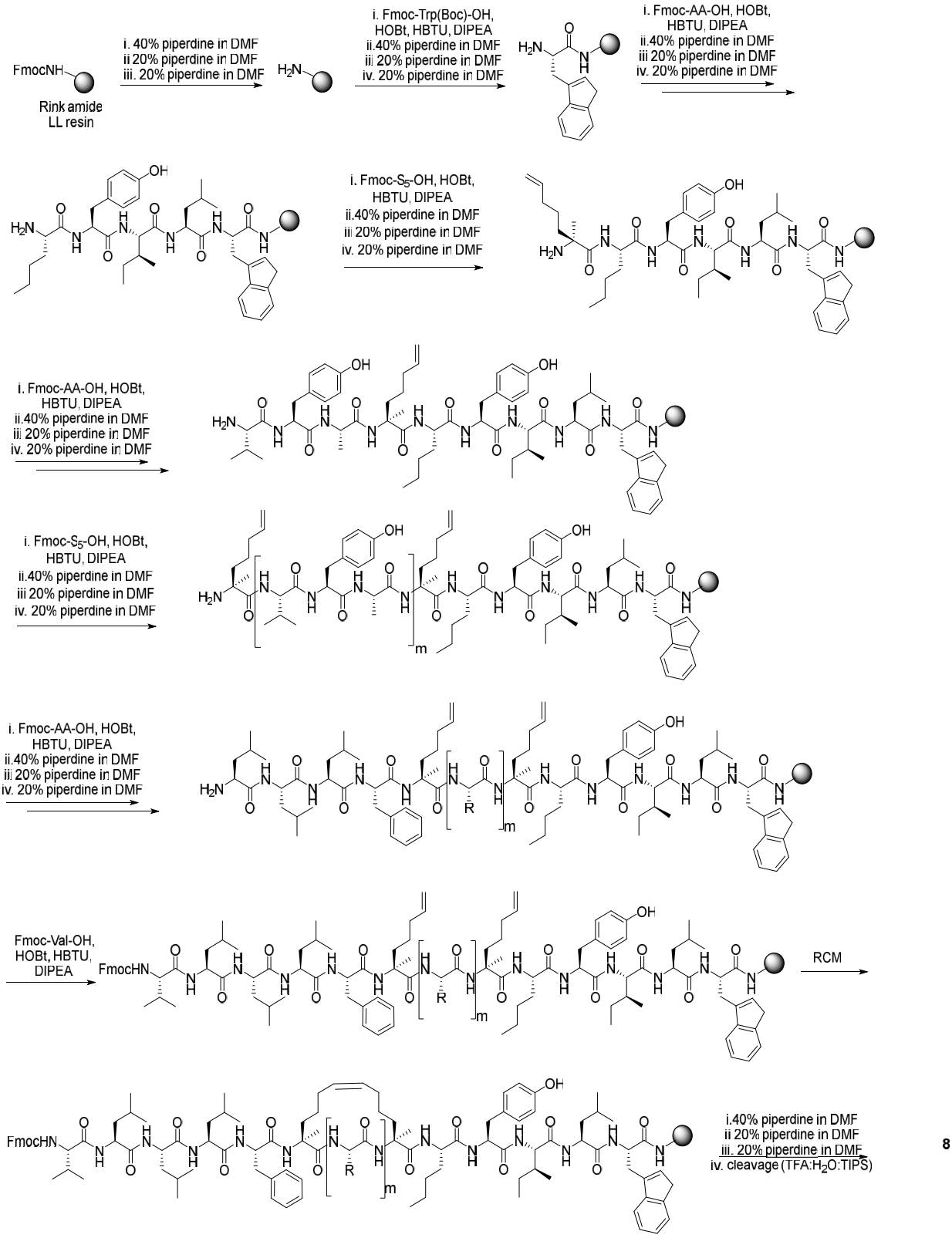

Scheme 2: Synthesis of stapled peptide 8.

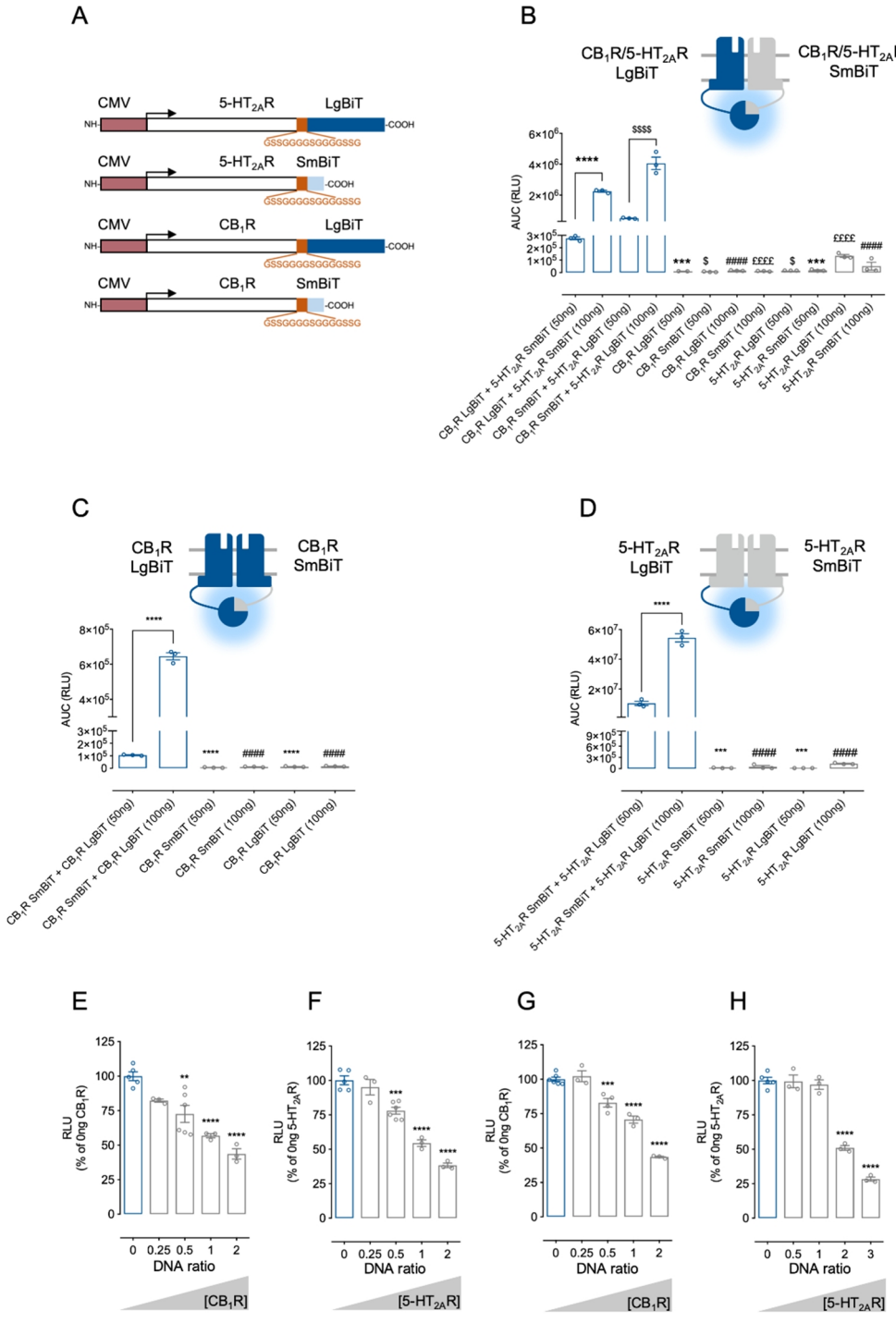
A
CMV
5-HT2AR
LgBiT
NH
COOH
GSSGGGGSGGGGSGGSG
CMV
5-HT2AR
SmBiT
CMV
CB1R
LgBiT
CMV
CB1R
SmBiT
B
CB1R/5-HT2AR LgBiT
CB1R/5-HT2AR SmBiT
AUC (RLU)
CB1R LgBiT + 5-HT2AR SmBiT (50ng)
CB1R LgBiT + 5-HT2AR SmBiT (100ng)
CB1R SmBiT + 5-HT2AR LgBiT (50ng)
CB1R SmBiT + 5-HT2AR LgBiT (100ng)
CB1R LgBiT (50ng)
CB1R SmBiT (50ng)
CB1R LgBiT (100ng)
CB1R SmBiT (100ng)
5-HT2AR LgBiT (50ng)
5-HT2AR SmBiT (50ng)
5-HT2AR LgBiT (100ng)
5-HT2AR SmBiT (100ng)
C
CB1R LgBiT
CB1R SmBiT
AUC (RLU)
CB1R SmBiT + CB1R LgBiT (50ng)
CB1R SmBiT + CB1R LgBiT (100ng)
CB1R SmBiT (50ng)
CB1R SmBiT (100ng)
CB1R LgBiT (50ng)
CB1R LgBiT (100ng)
D
5-HT2AR LgBiT
5-HT2AR SmBiT
AUC (RLU)
5-HT2AR SmBiT + 5-HT2AR LgBiT (50ng)
5-HT2AR SmBiT + 5-HT2AR LgBiT (100ng)
5-HT2AR SmBiT (50ng)
5-HT2AR SmBiT (100ng)
5-HT2AR LgBiT (50ng)
5-HT2AR LgBiT (100ng)
E
RLU (% of 0ng CB1R)
DNA ratio
[CB1R]
F
RLU (% of 0ng 5-HT2AR)
DNA ratio
[5-HT2AR]
G
RLU (% of 0ng CB1R)
DNA ratio
[CB1R]
H
RLU (% of 0ng 5-HT2AR)
DNA ratio
[5-HT2AR]

Figure 1. NanoBiT complementation can be used to estimate oligomer affinities. (A) Schematic representation of the CMV-promoter NanoBiT fusion proteins. HEK 293 cells were transiently transfected with all possible orientations of LgBiT and SmBiT C-terminal fusions at two different DNA ratios (50 or 100 ng receptor/well) to assess 5-HT_{2A}R-CB_1R heteromers **(B)** or CB_1R **(C)** and 5-HT_{2A}R **(D)** homomers. Disruption of CB_1R **(E)** and 5-HT_{2A}R **(F)** homomers and 5-HT_{2A}R-CB_1R heteromers **(G and H)** was assessed in the presence of increasing un-tagged receptor concentrations (see figure legends). In B-D, data are mean AUC (RLU) ± SEM (n = 3). In (B), statistical significance was evaluated by one-way analysis of variance (ANOVA) followed by Bonferroni post hoc tests showing significant effects for CB_1R LgBiT + 5-HT_{2A}R SmBiT (50ng) against the same configuration at 100 ng/well or each equivalent individual construct (***p ≤0.001, ****p ≤0.0001), for CB_1R LgBiT + 5-HT_{2A}R SmBiT (100ng) over each equivalent individual construct (####p ≤0.0001), for CB_1R SmBiT + 5-HT_{2A}R LgBiT (50ng) over the same configuration at 100 ng/well or each equivalent individual construct ($p≤0.05, $$$$p ≤0.0001) and for CB_1R SmBiT + 5-HT_{2A}R LgBiT (100ng) over each equivalent individual construct (££££p ≤0.0001). In C and D, statistical significance was evaluated as in B, showing significant effects for CB_1 SmBiT + CB_1R LgBiT (50) or 5-HT_{2A}R SmBiT + 5-HT_{2A}R LgBiT (50) over the same configuration at 100 ng/well or each equivalent individual construct (***p ≤0.001, ****p ≤0.0001) and for CB_1 SmBiT + CB_1R LgBiT (100) or 5-HT_{2A}R SmBiT + 5-HT_{2A}R LgBiT (100) over each individual construct (####p ≤0.0001). In E-H, values are mean ± SEM (n ≥ 3) of percentage of luminescence normalised to 0 ng of non-tagged competitor. For each condition, statistical significance was evaluated by one-way analysis of variance (ANOVA) followed by Bonferroni post hoc tests showing significant effects over 0 ng of non-tagged competitor (**p ≤0.01, ***p ≤0.001, ****p ≤0.001). CMV, human cytomegalovirus immediate-early promoter.

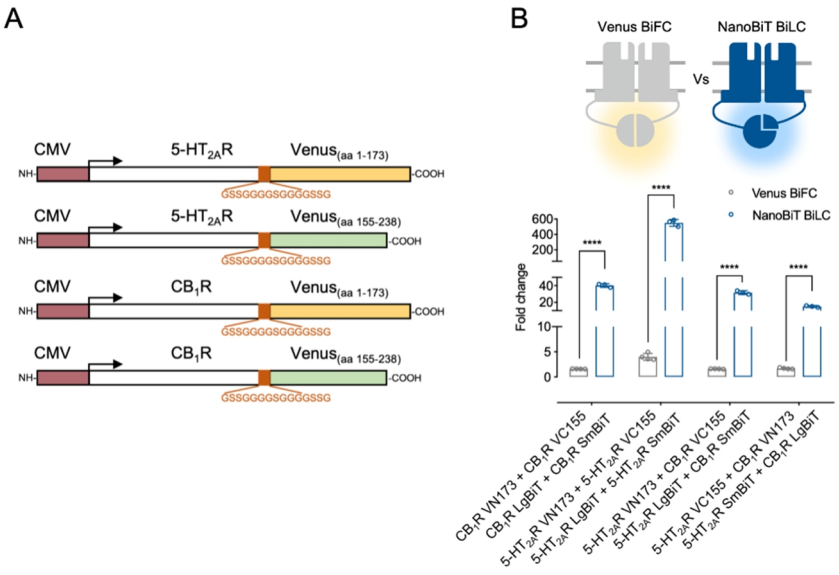

Figure 2. Comparative analysis of NanoBiT with Venus Bimolecular Fluorescent complementation (BiFC). (A) Schematic representation of the CMV-driven Venus YFP BiFC fusion proteins. In **(B)**, HEK-293 cells were transiently transfected with all possible Venus YFP complementary orientations and compared to its equivalent NanoBiT BiLC pairs to assess CB_1R and $5\text{-}HT_{2A}R$ homomers and $5\text{-}HT_{2A}R$-CB_1R heteromers. Data are mean ± SEM ($n \geq 3$) of fold change, calculated as ratio between each condition and the individual receptor construct with the highest luminescence/fluorescence values. Statistical significance was evaluated by unpaired t-tests between groups followed by Holk-Sidak corrections for multiple comparison (****$p \leq 0.0001$). CMV, human cytomegalovirus immediate-early promoter.

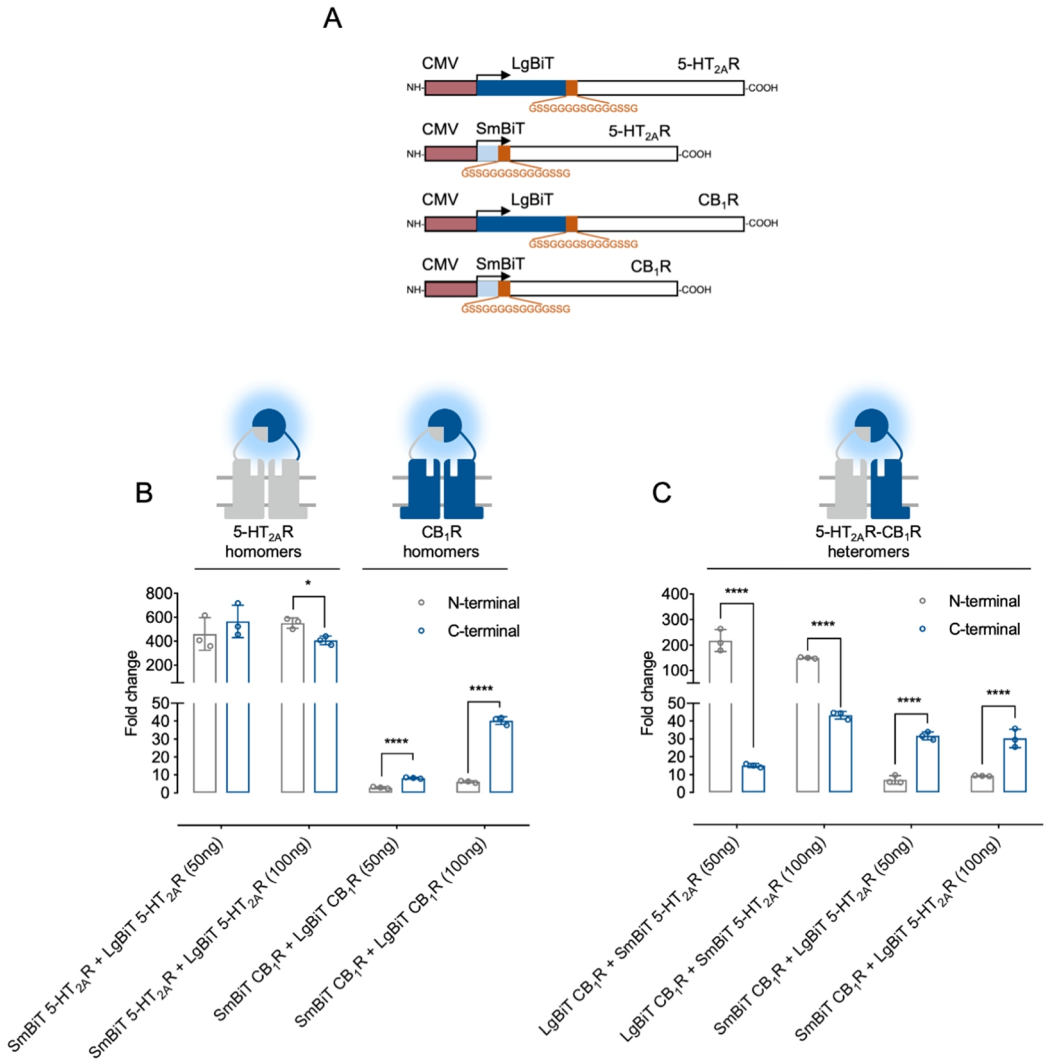

Figure 3. Assay optimisation for the screening of peptides disrupting 5-HT$_{2A}$R-CB$_1$R heteromers. **(A)** Schematic representation of the CMV-driven NanoBiT N-terminally tagged CB$_1$ and 5-HT$_{2A}$ receptors. Comparison between N-terminal or C-terminal tagging to assess CB$_1$R and 5-HT$_{2A}$ receptors homomers **(B)** or 5-HT$_{2A}$R-CB$_1$R heteromers **(C)**. Data are mean ± SEM (n = 3) of fold change, calculated as the ratio between each condition and the individual receptor construct with the highest luminescence background. Statistical significance was evaluated by unpaired t-tests between groups followed by Holk-Sidak corrections for multiple comparison (*p ≤0.05,****p ≤0.0001). CMV, human cytomegalovirus immediate-early promoter.

A

		Yield (mg)	R_t (min)	Purity (%)	$[M+H^+]$ calc.	$[M+H^+]$ Peak Found
TM7 $hCB_1R_{(374-400)}$	LIKTVFAFCSMLCLLNSTVNPIIYALR					
TM7-TAT	LIKTVFAFCSMLCLLNSTVNPIIYALRGRKKRRQRRR					
TM6 $hCB_1R_{(343-365)}$	KTLVLILVVLIICWGPLLAIMVY					
TM6-TAT	GRKKRRQRRRKTLVLILVVLIICWGPLLAIMVY					
TM5 $hCB_1R_{(273-299)}$	ETYLMFWIGVTSVLLLFIVYAYMYILW					
TM5-TAT	ETYLMFWIGVTSVLLLFIVYAYMYILWGRKKRRQRRR					
7	$VS_5LLFS_5VYAYN_LYILW$GRKKRRQRRR	nd	nd	nd	nd	nd
8	$VLLLFS_5VYAS_5N_LYILW$	1.2	20.6	93	1876.20	1876.77
9	$VYS_5YN_LS_5ILW$	2.1	18.0	97	1259.38	1259.41
10	$VYS_5YN_LYS_5LW$GRKKRRQRRR	4.6	15.8	96	2648.00	2648.60
11	$VYS_5YN_LS_5ILW$	0.5	18.1	100	1287.36	1287.44

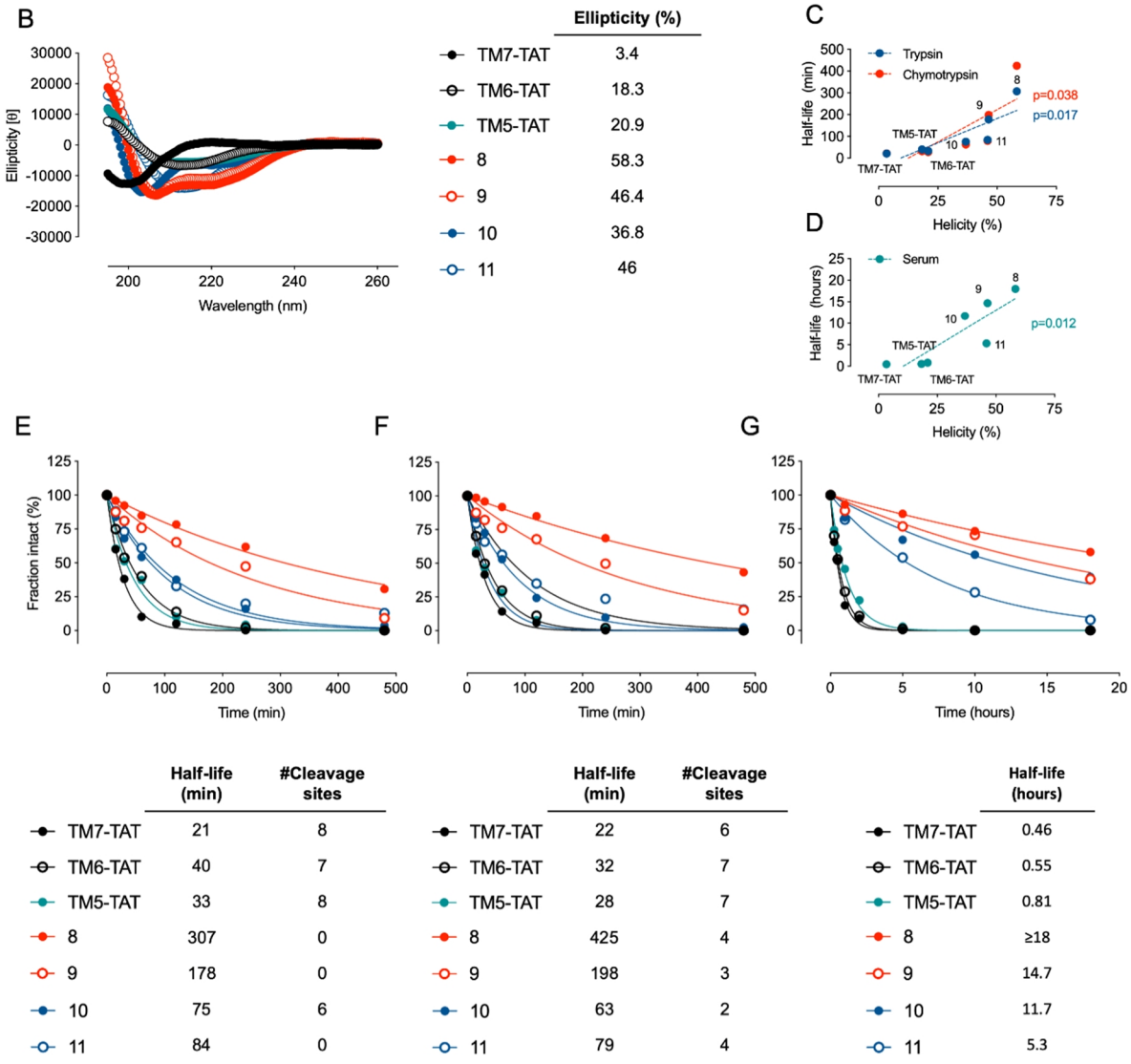

	Half-life (min)	#Cleavage sites
TM7-TAT	21	8
TM6-TAT	40	7
TM5-TAT	33	8
8	307	0
9	178	0
10	75	6
11	84	0

	Half-life (min)	#Cleavage sites
TM7-TAT	22	6
TM6-TAT	32	7
TM5-TAT	28	7
8	425	4
9	198	3
10	63	2
11	79	4

	Half-life (hours)
TM7-TAT	0.46
TM6-TAT	0.55
TM5-TAT	0.81
8	≥18
9	14.7
10	11.7
11	5.3

Figure 4. Biophysical Analysis of Stapled Peptides (A) Amino acid sequence alignment of the targeted TM regions and disrupting peptides. Cys are in reduced state. Blue bridges indicate the stapled amino acid residues. HIV-TAT amino acid sequence is displayed in red. Yields, purity and MALDI-TOF data shown for the stapled peptides and negative control. **(B)** Circular dichroism analysis of **30-50 µM** peptides at **20°C**. For proteolytic stability studies, the peptides solution (55.5 µM for trypsin and chymotrypsin and 11.1 µM for serum) were incubated in the presence of **0.55 µg/mL** of trypsin from porcine pancreas **(E),** α-chymotrypsin **(F**) or mouse serum **(G)** at 37 °C for the indicated times (see figure legends). Data are mean ± SEM (n = 3) percentage of intact peptide normalised to t=0. Proteolytic half-lives and putative cleavage sites (predicted using Expasy bioinformatics server's model with the 50% probability of cleavage) are indicated in the bottom panels of each figure. Positive correlation between helicity and half-life in trypsin/chymotrypsin **(C)** or serum **(D)** was determined by two-tailed Pearson's correlation test.

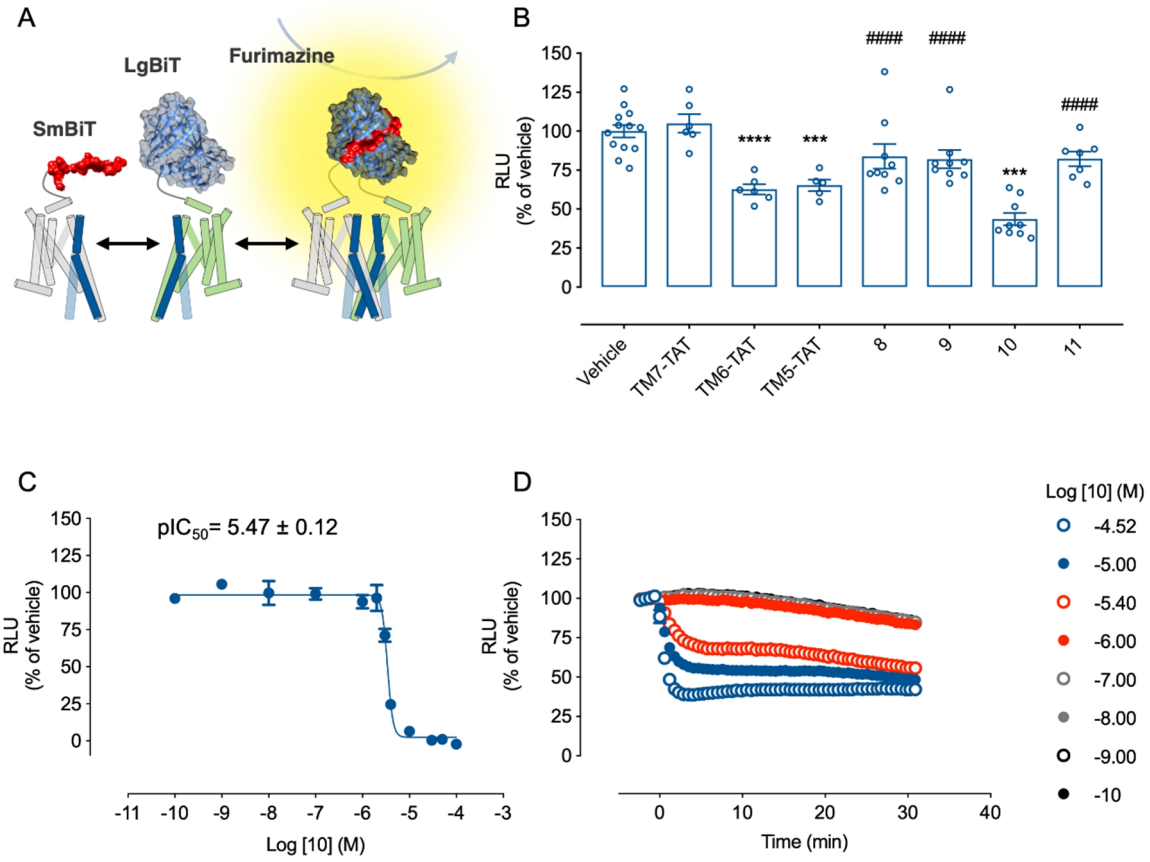

Figure 5. Identification of a small-stapled TM peptide disrupting 5-HT$_{2A}$R-CB$_1$R heteromers. (A) Schematic representation of the NanoBiT assay using N-terminally labelled constructs. In **(B)**, HEK-293 cells transiently expressing the LgBT-CB$_1$R and SmBiT- 5-HT$_{2A}$R complementary pairs were pre-incubated for 1h at 37°C with the indicated peptides (4 µM) or vehicle prior to luminescence recording. Data are mean RLU ± SEM (n ≥ 5) percentage of luminescence normalised to vehicle-treated cells. Statistical significance was evaluated by one-way analysis of variance (ANOVA) followed by Bonferroni post hoc tests, indicating significant differences over vehicle-treated cells (, ***p ≤0.001, ****p ≤0.0001) and for peptide 10 over its related peptides ($^{\#\#\#\#}$p ≤0.0001). Peptide 10 potency **(C)** was evaluated as in A over increasing peptide concentrations (see figure legends) (n=3). Alternatively, to assess the kinetics of the peptide 10-driven heteromer disruption **(D),** prior to the administration of the peptide (see figure legends), the cells were pre-incubated with substrate and the luminescence was recorded over the following 30 min. Data are mean RLU ± SEM (n ≥ 3) percentage of luminescence normalised to vehicle treated cells.